A survey of the continuous radiation at a frequency of 400 Mc/s

Seeger, C.L.; Westerhout, G.; Conway, R.G.; Hoekema, T.

1965, *Bull. Astr. Inst. Netherlands* **18** 11–41;
Communication from the Netherlands Foundation for Radio Astronomy and the Observatory at Leiden

A SURVEY OF THE CONTINUOUS RADIATION AT A FREQUENCY OF 400 Mc/s

Ch. L. SEEGER*, GART WESTERHOUT**, R. G. CONWAY† and T. HOEKEMA

Received 7 September 1964

In the spring of 1957, a survey was made of the sky between the north pole and declination $-35°$, using the 25-metre radio telescope at Dwingeloo. The distribution of the background emission over the sky is given in the form of contour maps (figures 12 and 16). Many difficulties were encountered in attempts to remove the large effects of radiation from the ground and the sky in the side-lobes (the beam efficiency $\eta_B = 0.56$). It is believed that the background level is accurate to $\pm$ 6 °K, and the relative temperature scale to $\pm$ 5 per cent. The flux density of Cas A (5600×10^{-26}) was used as an intensity standard. A comparison with the Cambridge survey at 404 Mc/s gave satisfactory agreement, and enabled us to determine an absolute zero-level. Ratios are given for the flux densities of the six brightest radio sources. The presence of a polarized component in the background, discovered after this survey was made and reduced, has no appreciable influence on the intensities given here. The galactic 'halo' shows many irregularities. It is suggested that these are the remains of older, broken-up arcs such as the 'spur' in the northern galactic hemisphere and the 'Cetus arc' in the south. The 'halo' might well be directly connected with the non-thermal emitters in the galactic plane and only extend to a few kpc above the plane. In an article immediately following this one, the flux densities of 149 sources are given.

Introduction

This article describes a survey of most of the sky above a declination of $-32°$, made at a frequency of 400 Mc/s with a beamwidth of $2°.2 \times 1°.7$. During November 1955 some observations were made of selected regions in the sky, while the receiver was installed in the telescope for the observation of the occultation of the Crab nebula by the Moon (SEEGER, WESTERHOUT and VAN DE HULST, 1956). These were followed by the present survey which was made in February, March and April, 1957.

In the observations and subsequent reductions, great care was taken to eliminate the effects of ground radiation in the side- and back-lobes of the antenna, so that it is possible to have some faith in the relative levels of the intensity in the low-intensity parts of the sky. No absolute measurements of the background intensity were made, so that the zero-level is unknown. It was obtained later from a comparison with the Cambridge survey (PAULINI-TOTH and SHAKESHAFT, 1962). The flux density of a number of discrete sources, taken from the second Cambridge catalogue (SHAKESHAFT *et al.*, 1955), was measured, and published together with some data on the Coma cluster, the Moon and the Andromeda nebula (SEEGER, WESTERHOUT and CONWAY, 1957). These sources are included in a list of 149 sources published in the following article (DAVIS, GELATO-VOLDERS and WESTERHOUT, 1965). For details on calibration of the optical and radio axis of the telescope we refer to WESTERHOUT (1958); the same procedure was followed in the present investigation. Technical details of the receiver are described by SEEGER, STUMPERS and VAN HURCK (1960). They also published a preliminary map, which is superseded by the present maps.

In section 1 the receiver and antenna system are described, and the results of the telescope and receiver calibrations are given. Section 2 describes the data used in the reduction, and in section 3 the reduction procedure is described and the data are presented in the form of maps in equatorial and galactic coordinates. A general discussion of the data is given in section 4.

The observations were made with the 25-metre paraboloidal mirror at Dwingeloo. The telescope is operated by the Netherlands Foundation for Radio Astron-

* Now at the University of Texas, Austin, Texas, U.S.A.
** Now at the University of Maryland, College Park, Md., U.S.A.
† Now at the Nuffield Radio Astronomy Laboratories, Jodrell Bank, Macclesfield, Cheshire, England.

omy, and is financed by the Netherlands Organization for the Advancement of Pure Research (Z.W.O.). All technical aspects of the investigation described in this paper are likewise financed by this Organization, whereas the reductions took place at the Astronomical Observatory of the University at Leiden. The receiver and antenna were installed during February, 1957, and a regular observing program was conducted between March 10 and May 1, 1957.

The construction of the receiver was directed by Seeger, partly at the Philips Laboratories in cooperation with F. L. H. M. Stumpers and N. van Hurck, partly at the Leiden Observatory, with the assistance of J. H. Kuypers. The observations were directed by Seeger and Westerhout and made by Seeger, Westerhout, Conway and Kuypers. The reduction was done mainly by Hoekema under the supervision of Westerhout, with the exception of the reductions described in sections 1.2 and 1.3 which were done by Conway. The present article and the delay in its publication are the responsibility of Westerhout.

1. Receiver and antenna calibrations

1.1. *Description of the instrument*

The receiver has been described in detail by SEEGER, STUMPERS and VAN HURCK (1959). We shall briefly describe here the main features of the system.

The antenna was a cylindrical waveguide section, about 65 cm wide and 90 cm long, with a probe entering from the side. It was supported by four aluminium pipes which, about 1 metre in front of the mouth of the waveguide, were attached to the two arms of an aluminium cross on top of a 12-metre mast. The mast was held by guy wires and fixed to the centre of the paraboloid. Although this type of feed in principle has very low spillover characteristics if properly designed, the structure in front of it caused a large amount of stray radiation and made the spillover and stray radiation 2.5 times worse than it should have been. The signal was fed through coaxial cable to the centre of the paraboloid, and then down to the rotating laboratory in the base of the telescope, where the receiver was installed. The rotation around the horizontal axis of the telescope was taken up by a rotary joint.

The receiver was a normal superheterodyne, with a high-frequency preamplifier employing two EC 57 disk-seal triodes in cascode and a gain of about 36 db. The crystal-diode mixer thus contributes very little to the system noise, and with a specially selected EC 57 for the first tube, the receiver noise temperature in the laboratory was 435 °K. The local oscillator was at 350 Mc/s, and the intermediate frequency 50 Mc/s. The image frequency was attenuated by 45 db. Supply voltages were kept constant to 1 part in 10^5 with the aid of a stabilizer using a standard cell as a reference. The observations were made with a bandwidth of 10 Mc/s, although 1 Mc/s could be used if necessary. A wide-band calibrated pushbutton attenuator was incorporated in the i.f. amplifier giving attenuation up to 20 db in steps of 1 db. The detector was followed by a very stable d.c. amplifier, provided with variable zero-offset, exactly calibrated gain steps, and time constants variable from 0.1 to 10 seconds; the observations were made with 1 second time constant. A Honeywell-Brown strip-chart recorder was used for recording the data.

In the laboratory, under constant-temperature conditions, the receiver gain varied by less than 1 per cent over periods of weeks. On the telescope, however, no temperature control was provided, and this together with the continuous shaking, motion of cables and rotary joints caused both large drifts and sudden gain and zero-level variations. As will be mentioned later, gain changes of up to 30 per cent occurred during the observing period, and changes of up to 5 per cent during any one night are suspected. The addition of long cables (35 metres between the antenna probe and the receiver, loss 1.09 db or a factor of 0.78), many connectors, and the rather large side-lobe radiation, increased the total noise temperature during the actual operation, measured at the antenna, to approximately 1100 °K. The total noise temperature was never directly measured, but was determined from the response to the source Cas A and the estimated antenna efficiency. It resulted in peak-to-peak fluctuations in the output of the order of 1 °K in antenna temperature or about 1.5 units in our scale.

1.2. *The linearity of the receiver response*

Most of the non-linearity of the receiver response is introduced at the detector stage, and this was measured by the method described by SEEGER (1956), i.e. by recording the deflections when a constant power at the

input was attenuated by known amounts. Power corresponding to room temperature was obtained from a matched load at the receiver input, and the signal was attenuated at the i.f. stage by 20 db in 1 db steps. This linearity check was repeated altogether four times during the period of observation, and it appeared that the response was effectively constant during that period.

It was found that the data could be fitted satisfactorily to an analytic function of the form

$$W = aE + bE^2 + cE^3 + dE^4,$$

where W is the input power and E the output reading. A correction factor p, which can be applied directly to the output readings, was calculated from

$$p = \left(\frac{dE}{dW}\right)_{E_0} (W - W_0)/(E - E_0),$$

where E_0 is the base level. Thus, the intensity with respect to the base level, ΔE, is related to the reading above the base level as $\Delta E = p(E - E_0)$.

All intensities in this article are expressed in 'units'; 1 unit = 0.5 mV. Assuming an average base level of 1200 mV, the formula for p becomes

$$p = 1 + 0.00006\,\Delta I,$$

where ΔI is the intensity of the source or background feature in our units. Variations in the base level between 1000 and 1400 mV introduce a maximum error of 20 per cent in the coefficient of ΔI. Since the highest intensities in the survey, with the exception of Cas A, Sgr A and Cyg A, have $\Delta I < 300$ units, $p < 1.018$; the maximum error in p is of the order of ± 0.005.

The intensities given in the maps were not corrected for the non-linearity of the receiver. As seen from the above, the corrections amount to 1.8 per cent or 5.4 units in the brightest parts of the Milky Way, $\Delta I = 300$ units. For $\Delta I = 100$ units, the correction is 0.6 units. In view of the other uncertainties, the correction can be neglected for most purposes.

1.3. *Antenna pattern*

The antenna pattern was measured on two consecutive days, by making sweeps in azimuth in a region $30° \times 20°$ around the Sun. It was decided to sweep in azimuth, rather than in right-ascension and declination; even though the Sun moved in the azimuthal coordinate system, reduction of azimuth sweeps to a map of the antenna pattern of an azimuthally mounted telescope is easier than converting each sweep in right-ascension. The coordinate transformer was set to the position of the Sun, and the telescope was made to follow the Sun in elevation, while a sweep was made in azimuth. This sweep is thus a true horizontal cross-section. At the point at which the telescope passed the exact position of the Sun given by the coordinate transformer, the azimuth error indicator went through zero and a marker was put on the record. Similar sweeps were then made with the coordinate transformer's position moved in steps of 0°.5 in declination. The point at which the azimuth equals the azimuth of the coordinate transformer is not at the same azimuth as the Sun, but the Sun's azimuth can be found immediately from the difference in declination and the position angle of this point at the Sun. A small table was calculated for this purpose, which also gave the length of a degree on the sky in each sweep, taking into account the motion of the Sun in azimuth during the sweep and the average elevation of the sweep. After drawing a zero-line through the 5 degrees at the two ends of the sweep, the recorded curve could be read off, giving intensities directly in a rectangular coordinate grid centered on the Sun. Since the full-beam brightness temperature of the Sun was of the order of 36000 °K or 30000 units of our contour map, confusion with background features started at a level of about 0.03 per cent of the Sun's intensity (9 units; the Sun was in an empty part of the sky). Close to the Sun, the recorder zero was lowered, which could be done in 10 calibrated steps of exactly one full scale each. The top intensity of the Sun was measured several times during the day to guard against variations. The region close to the Sun was measured separately with reduced sensitivity of the d.c. amplifier.

The intensities were corrected for the non-linearity of the receiver and expressed in per cent of the maximum intensity. A contour map down to 0.05 per cent was then constructed (figure 1). Accurate cross-sections in the horizontal, vertical and diagonal directions are presented in figure 2. A few near-in side-lobes between 0.3 and 5 per cent are present, probably caused by the feed support and the guy wires. The patterns in figures 1 and 2 are not corrected for the Sun's angular size, and have half-power widths of 2°.22 in the magnetic and 1°.73 in the electric (vertical) plane. This correction

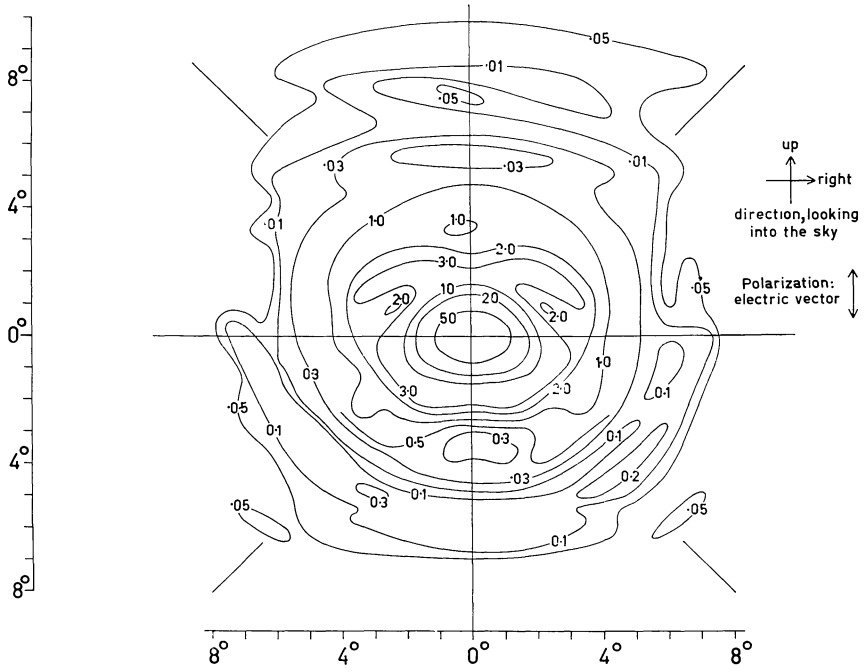

Figure 1. Antenna pattern, uncorrected for the diameter of the Sun. Contour numbers are per cent of the sensitivity along the axis.

only amounts to about 2 per cent, and we shall adopt for the half-power widths the values $2°.2 \times 1°.7$. The principal patterns are Gaussian down to the 10 per cent level, and if the beam were entirely Gaussian, the beam solid angle (see section 1.4) would be 4.24 square degrees, where the area enclosed by the 0.05 per cent contour is defined as the full beam. The data on the full beam, derived here, are summarized in section 1.4 below, together with other antenna and receiver parameters, and definitions of terms.

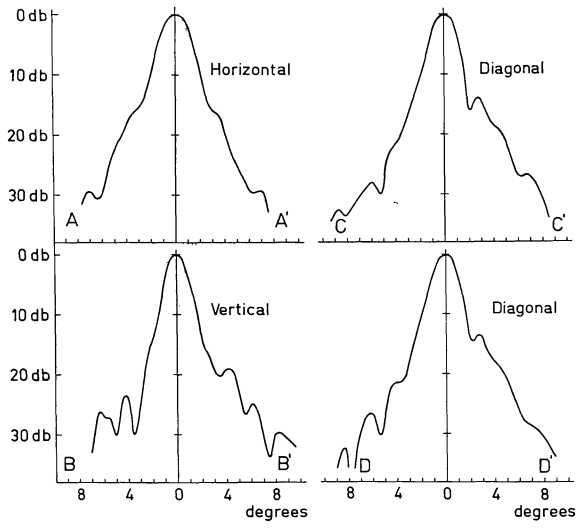

Figure 2. Cross-sections through the antenna pattern.

1.4. *Intensity calibration*

We start this section with a general definition of the quantities determining the characteristics of an antenna and their interrelations, expanding somewhat the definitions given earlier by SEEGER *et al.* (1956) and WESTERHOUT *et al.* (1962).

$f(\theta, \varphi)$ Antenna pattern, power response to a randomly polarized wave of the antenna in the direction (θ, φ) relative to the maximum response $f(0,0) = 1$ [$f(\theta, \varphi)$ is given in per cent in figure 1].

Full beam The part of the antenna pattern down to a level necessary for the problem under consideration. In this paper, the full beam contains the first side-lobes out to about 8 degrees from the axis.

Ω Antenna solid angle, integral of the antenna pattern over the sphere.

$$\Omega = \int_{4\pi} f(\theta, \varphi)\, d\Omega .$$

Ω' Beam solid angle, integral of the antenna pattern over the full beam. If the full beam is exactly Gaussian down to zero, $\Omega' = 1.133\ \theta_E\theta_H$, where θ_E and θ_H are the half-power widths in the electric and magnetic planes.

D Directivity, ratio of maximum antenna power response to average power response over all directions. $D = 4\pi/\Omega$.

D' Beam directivity, ratio of maximum antenna power response to average power response over all directions if $f(\theta,\varphi)$ were zero outside the full beam. $D' = 4\pi/\Omega'$.

G Forward antenna gain, ratio of maximum antenna power response to the power response of a lossless isotropic antenna with identical impedance.

$$G = \eta_R D = (1-\beta)\eta_R D' .$$

η_R Radiation efficiency, ratio of the available power at the antenna terminals to the total power absorbed by the antenna. (Available power is the output power from the antenna terminals into an impedance which is adjusted for optimum power transfer [matched]). It specifies the losses in the receptive element and the reflector surface which in general are difficult to measure. It does not include the easily measurable loss in the receiver cable.

β Stray factor, fraction of the total power which the antenna would absorb in an isotropic radiation field, incident from directions outside the full beam (diffraction sidelobes, scattering against feed and feed supports, spillover, and radiation through the reflecting screen).

$$\beta = 1-\Omega'/\Omega = 1-D/D' .$$

η_B Beam efficiency, fraction of the total power, incident from the full beam, which is available at the antenna terminals.

$$\eta_B = (1-\beta)\eta_R = \frac{G}{4\pi}\Omega' = \frac{G}{D'} = \frac{A}{\lambda^2}\Omega' .$$

A Effective area of the antenna, defined by $A = \lambda^2 G/4\pi$. The available power per unit bandwidth at the antenna terminals from an unpolarized wave of flux density S is $\frac{1}{2}SA$.

η_A Antenna efficiency, ratio of effective area to geometrical area, or of actual gain to maximum possible gain (with uniformly illuminated aperture).

$$\eta_A = A/A_g = G\lambda^2/4\pi A_g = \eta_B\lambda^2/A_g\Omega' .$$

T_b Brightness temperature in a particular direction, temperature of a black body situated in that direction for which the brightness of the thermal radiation would equal the observed brightness, B.

$$T_b = \lambda^2 B/2k .*$$

$\overline{T}_b$ Full-beam brightness temperature, weighted mean of the brightness temperature over the full beam.

$$\overline{T}_b = \frac{1}{\Omega'}\int_{\text{full beam}} f(\theta, \varphi) T_b(\theta, \varphi)\, d\Omega ,$$

T_A Antenna temperature, absolute temperature of an impedance, identical to the antenna impedance which, if connected in place of the antenna, would deliver the same available noise power to the antenna terminals as the antenna.

$$T_A = \frac{\eta_R}{\Omega}\int_{4\pi} f(\theta, \varphi)\, T_b(\theta, \varphi)\, d\Omega =$$

$$= \frac{\eta_B}{\Omega'}\left[\int_{\text{full beam}} f(\theta,\varphi)\, T_b(\theta,\varphi)\, d\Omega + \int_{\text{sphere-full beam}} f(\theta,\varphi)\, T_b(\theta,\varphi)\, d\Omega\right].$$

If the last term is constant over a measurement,

$$T_A = \eta_B \overline{T}_b + \text{constant}.$$

* The Rayleigh-Jeans approximation is used throughout. It should be noted that at very high frequencies (mm waves) this very often does not hold. There, either the definition should read: 'A unit of brightness related to the surface brightness B as $T_b = \lambda^2 B/2k$' or the Planck formula should be used. The latter is the correct way to relate T_A to T_b, brightness and flux density. The definition of A and related quantities is likewise affected.

Neither a calibration of antenna temperature or total receiver noise, nor a complete determination of the antenna pattern was made. Therefore, the only quantity which can be used with some confidence is the beam solid angle Ω'. However, using the flux density of the source Cas A determined earlier (SEEGER, 1956), it is possible to find a relation between the full-beam brightness temperature $\overline{T}_b$ and the arbitrary scale of 'units' in which all our data are expressed. The flux density from a source which is small compared to the beamwidth may be written as

$$S = \int_{\text{source}} \frac{2k\,T_b}{\lambda^2}\,d\Omega = \frac{2k}{\lambda^2}\,\overline{T}_b\Omega'.$$

The same recorder deflection would be obtained from such a source or from an extended region with a full-beam brightness temperature $\overline{T}_b = S\lambda^2/2k\Omega'$. Assuming a flux density of 5600×10^{-26} watt$\cdot$m$^{-2}\cdot$(c/s)$^{-1}$ and noting that the recorder deflection for Cas A with respect to its immediate surroundings, corrected for alinearity, was 591.5 units (section 4.2) we find that $\overline{T}_b$ (Cas A) = 710 °K in $\overline{T}_b$.

It should be remarked that this conversion only holds for regions which occupy a small fraction of the sky. If the area is so large that $\int f(\theta, \varphi)d\Omega$ over the area becomes considerably greater than Ω', i.e., if the 'source' is very much larger than the full beam, the relation $T_A = \eta_B\overline{T}_b$ does no longer hold. The value of the proportionality factor η_B increases from 0.56 adopted here to values closer to unity, when the size of the region concerned increases. Our units are really units of T_A, but because of lack of calibration data, we have to express them in T_b. Differences between the intensities of neighbouring regions not larger than perhaps 30 to 50° across, such as the galactic ridge, the 'spur' at $l^{II} = 32°$ and many of the features in the emptier parts of the sky, are properly expressed in $\overline{T}_b$ using the conversion from units to $\overline{T}_b$ above. But the overall brightness temperature of the large low-intensity regions is likely to be lower by perhaps 20 or 30 per cent than the use of the conversion factor would indicate.

We shall now try to estimate the other antenna parameters. In section 2.3 a rough estimate is made of the value of $f(\theta, \varphi)$ in a hypothetical ring-shaped spillover lobe between about 90° and 125° from the forward direction, causing the sharp increase in side-lobe radiation between elevations 40° and 90° described there (see figures 6 and 7). It was found that, over 8000 square degrees, $f(\theta, \varphi) = 0.019$ per cent or 37.2 db below the sensitivity in the forward direction. In order to find Ω, we must add all the side-lobe contributions

$$\Omega = \Omega' + \int_{\substack{\text{sky-}\\ \text{full beam}}} f(\theta, \varphi)\,d\Omega.$$

During the day, sweeps in all parts of the sky showed spurious sources and increases in the background level of several °K, clearly due to radiation from the Sun in the side-lobes. With $\overline{T}_b$ (Sun) = 36000 °K (section 1.4), this indicates that the average side-lobe level is somewhere near 40 or 41 db, or $f(\theta, \varphi)$ between 10^{-4} and 0.8×10^{-4}. If this holds over the entire sky, apart from the ring-lobe, these side-lobes occupy 33000 square degrees. The value of the part of the antenna solid angle outside the full beam thus becomes $(1.9\times10^{-4}\times8000) + (0.8\times10^{-4}\times33000) = 4.16$ square degrees, and $\Omega = 5.28 + 4.16 = 9.44$ square degrees. This gives $\beta = 1 - \Omega'/\Omega = 0.44$. It is clear that this is only a very rough estimate, but the intensity of the solar radiation in the side-lobes, the large effect of the side-lobe radiation from the ground and the construction of the feed support all indicate that β should be larger than the theoretical value.

The latter can be calculated using the antenna pattern of this type of feed measured by CUTLER (1947). He only gives the pattern out to 90°, but it is likely that the sensitivity beyond 90° is extremely low (30 db in the backward direction). We find that the fraction of the radiation from the feed missing the paraboloid, i.e., between 55° and 180° from the axis of the feed, is 0.17. Assuming a perfect dish, all radiation falling on the dish goes into the full beam, and thus $\beta = 0.17$. It may thus be seen that the antenna efficiency is smaller than theoretical by a factor

$$(1-\beta)/(1-\beta_{\text{theoretical}}) = 0.67.$$

We can now calculate the other antenna parameters, and the results are summarized below. We have set $\eta_R = 1$ for convenience; it will probably not differ much from this value. It should be emphasized again that the values of Ω, D, G, η_B, η_A, A and T_A depend on the very rough estimate of β made above, and are not used in the reductions.

$\theta_H = 2°.2$
$\theta_E = 1°.7$
$\Omega' = 5.28$ square degrees
Ω' (Gaussian beam) $= 4.24$ square degrees
$\Omega \approx 9.44$ square degrees
$D' = 7810$
$D = G \approx 4370$
$\beta \approx 0.44$
$\eta_B \approx 0.56$
$\eta_A \approx 0.40$
$A \approx 196$ m^2
1 unit $= 1.20$ °K in $\overline{T}_b$
≈ 0.67 °K in T_A
$= 9.47 \times 10^{-26}$ watt · m^{-2} · (c/s)$^{-1}$ in S for a point source.

1.5. *Determination of the radio axis*

The radio axis is defined as the direction of maximum gain, and is intended to be identical with the optical axis of the paraboloid. The telescope is alt-azimuth mounted, and equatorial coordinates are converted into azimuthal coordinates by means of a mechanical coordinate transformer, which has a conversion accuracy of $\pm$ 0°.01. The optical axis was determined nine months before (WESTERHOUT, 1958) and the servo system made its azimuth and elevation coincide to within $\pm$ 0°.03 with the true coordinates corresponding to the right-ascension and declination setting of the indicator scales.

The position of the radio axis was determined by measuring the apparent positions of known radio sources and comparing these with the best-known positions. The latter are given in table 1. Sweeps were made through these sources in right-ascension and declination, and the differences $\Delta\alpha$ and $\Delta\delta$ between measured and true coordinates were then converted into ΔAz and Δh, the deviation in azimuthal coordinates. The conversion was made with the aid of a large-scale coordinate conversion grid on which the parallactic angle ψ could be measured easily. Later, a table was prepared on an electronic computer, giving Az, h and ψ as a function of hour angle and δ and vice versa. The mast supporting the antenna in the focus was adjusted a few months earlier, when a 21-cm continuum receiver was installed, to coincide with the optical axis. It turned out that the 75-cm antenna was mounted such that the 75-cm focus coincided to within 0°.02 with the 21-cm focus, so that no subsequent adjust

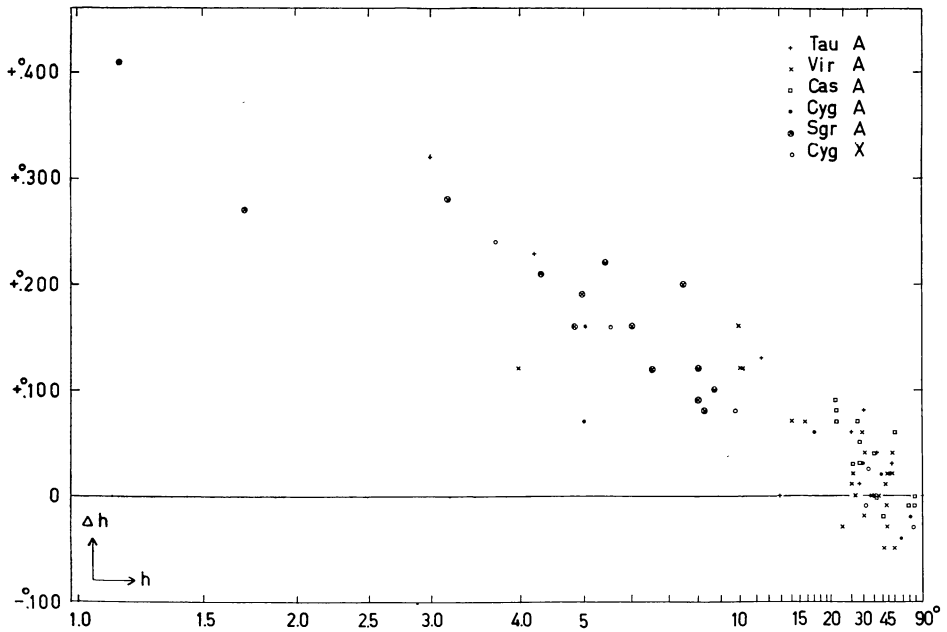

Figure 3. Deviation Δh from the standard position of radio stars. The scale of abscissae is chosen so as to make the optical refraction curve a straight line.

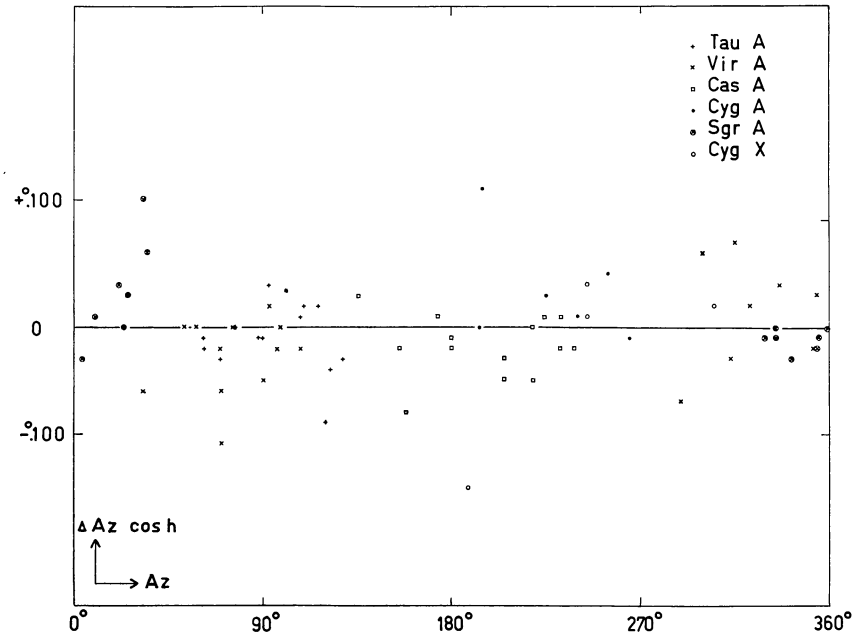

Figure 4. Deviation $\Delta Az \cos h$ from the standard position of radio stars.

ment of the mast was necessary. The results of the measurements are given in figure 3, where Δh is plotted as a function of h and in figure 4, where $\Delta Az \cos h$ is plotted as function of Az. The scale of h is chosen so that the optical refraction curve is a straight line. It may be seen that the points follow the optical refraction curve quite accurately; the probable error per point of the deviation is $\pm$ 0°.03. The points for Tau A are systematically higher by about 0°.03. This may be due to a cumulative error in the gears of the coordinate transformer at the declination of Tau A. The effect was not further investigated.

The position of Cyg X was initially determined only roughly, and the values of $\Delta Az \cos h$ and Δh deviated systematically from the average of the other points. After an adjustment of the coordinates to the values given in table 1 the points were made to agree, so that the position given is really a position determined during this survey. Cyg X was chosen as a calibrator because it is an extended source and thus the effects of scintillation, which often interfered seriously with the position measurements of the point sources, are very small. The position of Sgr A was taken from WESTERHOUT's (1958) 1390 Mc/s measurements and is seen to be in satisfactory agreement with these. We may conclude that radio refraction at 400 Mc/s is the same as optical refraction, and that the effects of bending of the mast supporting the antenna and deformation of the dish are negligible.

The plot of $\Delta Az \cos h$ versus h shows four points deviating from the mean by more than 0°.1. Three of these, at Az = 70°, 190° and 195° are probably due to the effects of scintillation. The measurements give an indication of a sinusoidal variation with an amplitude of about $\pm$ 0°.03, similar in phase and amplitude to the variation found in the calibrations of the optical

TABLE 1

Position of six bright radio sources, used in the calibration

Source	α (1950)	δ (1950)	α (1957)	δ (1957)
Tau A	$5^h31^m31^s$	+21 58′.9	82°.99	+21°.99
Vir A	12 28 18	+12 40.1	187.16	+12.63
Sgr A	17 42 43	−28 55*	265.79	−28.94
Cyg A	19 57 44	+40 35.8	299.50	+40.62
Cyg X	20 21 17	+40 22	305.38	+40.38
Cas A	23 21 11	+58 31.9	350.38	+58.57

* A better position for SgrA to be used with beamwidths of 0°.5 and larger, is recommended by I.A.U. Comm. 33b (GUM and PAWSEY, 1960): $17^h42^m37^s$, −28°57′ (1950).

axis and the radio axis at 1390 Mc/s, probably originating in one of the driving gears of the telescope. The probable error per point is about $\pm$ 0°.03. It is interesting to note that the present observations prove that it is possible to measure the position of a bright source, using a beamwidth of 2°.2, with a probable error of $\pm$ 0°.03, which is about 1.5 per cent of the beamwidth.

After correction has been made for refraction, the setting accuracy of the telescope at 400 Mc/s is $\pm$0°.03 (p.e.).

2. Data used in the reduction

2.1. *Receiver gain*

Throughout the observing period, the total receiver gain was checked by measuring the intensity of the sources Vir A, Tau A and Cas A with respect to comparison regions some 7 degrees away. The positions of the comparison regions are given in table 2. The measurements were made in the following way. The antenna was pointed at the source after applying the necessary refraction corrections, guiding on the source for one minute, and then changing the right-ascension or declination or both, repeating this once or twice, and then changing to comparison region A and guiding on that for one minute. On the average five measurements were made per night (observations were only made while the Sun was below the horizon). In order to be able to reduce all measurements to a common scale, the intensities of Cas A and Tau A were reduced to that of Vir A, and the values so obtained were plotted as a function of time for the observing period. The ratio of the intensities of Cas A and Tau A to that of Vir A was determined by taking weighted means of the ratio (source−comp.)/(Vir A−comp.) over 24 two-day periods (see section 4.2). Almost all the measurements were made above $h = 25°$, where extinction corrections are negligible compared to the accuracy of the measurements.

Since the intensity of Vir A was close to 50 units, this was taken as the standard intensity. All measurements are thus reduced to a sensitivity at which the intensity of Vir A with respect to its comparison region A is 50 units. The gain fluctuated slowly by about 12 per cent around the average.

In the first two weeks the gain was set more or less arbitrarily every day, causing day-to-day changes of 15 per cent or more. During the remaining six weeks the receiver gain settings were left untouched, and the gain decreased over that period regularly by about 6 per cent per week, except for two instances where tubes were changed. There was some indication of a regular decrease of the gain by about 5 per cent during the night and a subsequent increase during the day. The observing period was divided into intervals within which the gain did not change by more than 5 per cent, and the gain correction factor was assumed to be a constant during those intervals. Thus, the internal agreement in the scale of the reduced records is considered to be better than 5 per cent.

2.2. *Extinction*

A serious attempt was made to measure the extinction in the earth's atmosphere. This attempt was largely ineffective due to scintillation of most of the sources at low altitudes, and rapid gain and zero-line variations of the receiver at times.

If the extinction factor in the zenith is p and the equivalent air mass traversed at zenith distance z is $F(z)$, we have

$$I(z) = I(0)p^{F(z)-1},$$

where $I(z)$ is the intensity of the source at zenith distance z and $F(0) = 1$. The values of $F(z)$ were taken from the *Handbuch der Astrophysik* (SCHOENBERG, 1929). A series of measurements of $I(z)$ at different z permits us to determine p from

$$\log p = \frac{\mathrm{d} \log I(z)}{\mathrm{d}\, F(z)}.$$

The extinction in the zenith, expressed in decibels, may be written as $-10 \log p$, and the extinction at zenith distance z is $10\,[1-F(z)] \log p$, expressed in db over the extinction in the zenith. Since $\log p$ is expected to be of the order of -0.0040, it may be seen that the extinction at an altitude of 4°.2, where $F(z) = 12$, is expected to be of the order of 10 per cent. Thus, short-time gain variations of this order will completely spoil any measurement. Variations of at least 5 per cent occurred on most days.

The measurements were made by comparing the difference in intensity between a bright source and one or two comparison fields nearby, at different altitudes. The sources used and their comparison fields are given in table 2.

TABLE 2

Calibration sources and their comparison fields

Source	Source position		Comparison field A		Comparison field B	
	α (1957)	δ (1957)	α (1957)	δ (1957)	α (1957)	δ (1957)
Tau A	82°.99	+21°.99	75°.50	+21°.99	90°.00	+21°.99
Vir A	187.16	+12.63	180.00	+12.63	195.00	+12.63
Sgr A	265.79	−28.94	250.00	−28.94	281.00	−28.94
Cyg A	299.50	+40.62	290.00	+40.62	302.00	+40.62
Cyg X	305.35	+40.45	290.00	+40.45	320.00	+40.45
Cas A	350.38	+58.57	340.00	+58.57	1.00	+58.57

Before setting on the source, refraction corrections were applied to the position. Since, particularly at low altitudes, the altitude of the comparison field differs appreciably from that of the source, the intensity of each comparison field was corrected for the difference in radiation from the ground and the air between it and the source (section 2.3).

A total of 195 measurements were made in two periods of four consecutive nights, each consisting of a measurement of the source intensity and that of one or both of the comparison fields. The average intensity difference between the two comparison fields was determined from all measurements of one source, and the final intensities were given as I (source − comparison field A). It may easily be seen that if source a and source b are each measured twice at different zenith distances z_1 and z_3, and z_2 and z_4, respectively, then

$$\log p = \frac{\log I_a(z_1) - \log I_b(z_2) - \log I_a(z_3) + \log I_b(z_4)}{F(z_1) - F(z_2) - F(z_3) + F(z_4)},$$

which is independent of the actual ratio of the source intensities at $z = 0$.

It was soon found that the values of $\log p$ determined in this way were completely random, mainly due to large intensity variations arising from scintillation, and sometimes due to gain and zero-line variations. Even an attempt to find $\log p$ from 12 double pairs of measurements, where $I_a(z_1)$ and $I_b(z_2)$, and likewise $I_a(z_3)$ and $I_b(z_4)$ were measured within 30 minutes to eliminate gain variation, yielded values ranging from $-10 \log p = -0.204$ to $+0.067$. The reason for this became clear when the values of I for the various sources were plotted against time. Particularly at the lower altitudes, rapid changes in I of over 10 per cent occurred frequently, and it is these low altitudes which have most weight.

The only possible way of obtaining a reasonable result was taking all points together, after reducing the intensities of the various sources to a common value at high altitudes and applying the average day-to-day gain corrections. The result is given for five of the six sources in the top part and for Sgr A in the bottom part of figure 5. In the case of the five sources the spread is considerable. The spread in the points for Sgr A is considerably smaller. This must be due to the fact that it is an extended source and thus not so strongly influenced by scintillation. Also, our measurements and 1390 Mc/s measurements (WESTERHOUT, 1958) showed that the scintillation in the southern part of the sky is much weaker than in the north, where all low-altitude measurements of the other sources were made, and often entirely absent.

Values for $\log p$ were calculated by the method of least squares from the equation

$$\log I(z) - \log I(0) = [F(z) - 1] \log p$$

for the 152 observations of the five bright sources and the 43 observations of Sgr A separately. The results are given, together with the value found from 21-cm line measurements, in table 3.

It was recently shown by ALTENHOFF (1962, p. 31) that due to differential refraction sources which are of the same order of size as the antenna beam or larger, are seen too bright at low altitudes, thus reducing the effect of the extinction. He calculated corrected values for our 400 Mc/s observations, WESTERHOUT'S (unpublished) 1420 Mc/s observations and his own observations at 2700 Mc/s. These are given in the last column of table 3. In our reductions, we used the uncorrected value for Sgr A; this resulted in intensities

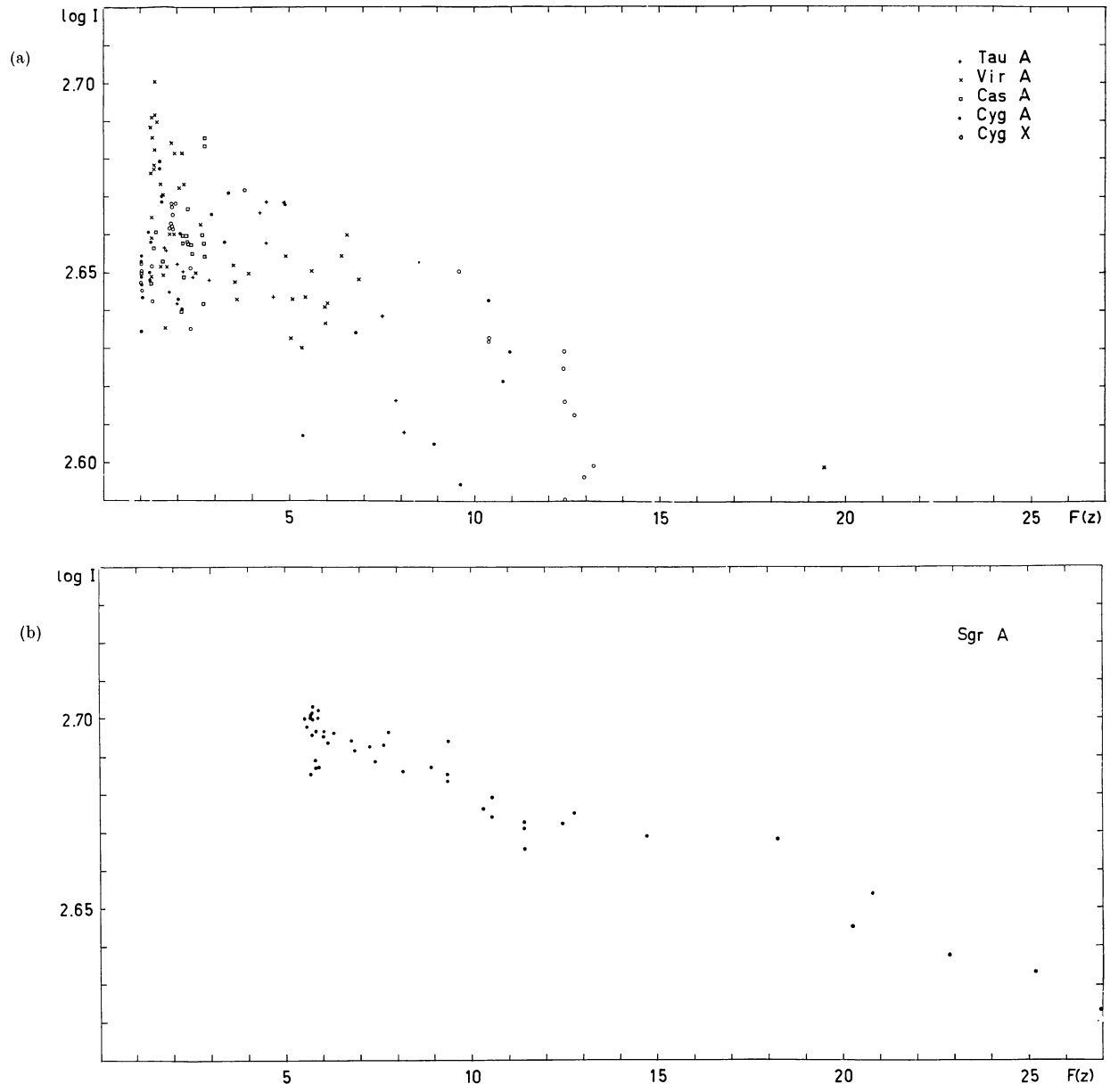

Figure 5. Intensities of six bright sources as a function of equivalent air mass, for determination of extinction: a) Four point sources and Cyg X, measured in the northern sky, b) Sgr A, measured in the southern sky.

which are too low by 1 per cent at 10° elevation and 2 per cent at 5° elevation. This error is negligible compared to other errors.

The agreement of Altenhoff's corrected values with theory is satisfactory, although it seems worth while to study in detail the question of extinction and scintillation by making numerous observations at a number of different frequencies.

2.3. *Radiation from the ground and the air*

In order to be able to provide a common zero-level for all measurements, a large number of declination sweeps were made at intervals of 30° in right-ascension. They were made in the form of sweeps in elevation close to the meridian. While the telescope moved slowly in azimuth, the elevation was changed from 0° to 70° or 90° with a speed of about 18° per minute. The timing

TABLE 3
Determination of the extinction

	Extinction in zenith ($-10 \log p$) (db)	p	Extinction corrected for differential refraction (db)	Freq. (Mc/s)
Average for five sources, setting in northern half of sky	0.0457 ± 0.0018	0.9895 ± 0.0004	0.046	400
Value for Sgr A, setting in southern half of sky	0.0345 ± 0.0010	0.9921 ± 0.0003	0.046	400
Value found at 1420 Mc/s (WESTERHOUT, unpublished)	0.0404 ± 0.0023	0.9907 ± 0.0006	0.06	1420
Value found at 2700 Mc/s (ALTENHOFF *et al.*, 1962)			0.095	2700

was such that the highest point was reached at the moment the azimuth was zero and the sidereal time was equal to the right-ascension concerned. After the highest point was reached, the sweep was repeated in the opposite direction. Figure 6 shows a sample recording. Immediately afterwards, the telescope was pointed to the celestial North Pole, to provide a reference level. The number of complete sweeps at any one right-ascension varied from 2 for $\alpha = 60°$ to 19 for $\alpha = 210°$. For each right-ascension, average curves were formed by plotting the measured intensities on transparent graph paper after correction to standard receiver gain, shifting the curves so obtained in the intensity-direction to make them coincide and drawing an average curve by hand. This graphical method was necessary because the North Pole intensities varied from one measurement to the other by amounts up to 5 or 10 units. This was due to shifts in the receiver zero while the telescope was being pointed to the North Pole, using the fast motion. Thus, even though an average North Pole level was calculated for each average curve, these levels cannot be very certain.

All average curves had the same general shape, as shown in figures 6 and 7. The intensity decreased sharply when the elevation increased from zero and the main beam and near-in side-lobes left the ground and the thick layer of air close to the horizon. The intensity then leveled off, to start rising again at roughly 40° elevation to a maximum near the zenith. Since many of the curves pass through relatively cold regions of sky, it seemed reasonable to assume that the lower envelope of all of them is the curve representing the radiation from the ground and the air in the main lobe and all side- and back-lobes. This lower envelope was again obtained graphically, by using the average North Pole level of each average curve as a zero. A number of average curves was discarded: a) $\alpha = 30°$ and 330° because they were taken in the daytime and showed solar interference, and were based on only three and four measurements, respectively. b) $\alpha = 60°$, 90° and 30° because they were based on two or three measurements only. It then turned out that $\alpha = 240°$ and 270° could hardly be used either, because they contained a large amount of Milky Way radiation. The final curve thus is based principally on the 56 measurements leading to the average curves for $\alpha = 120°$, 150°, 180°, and

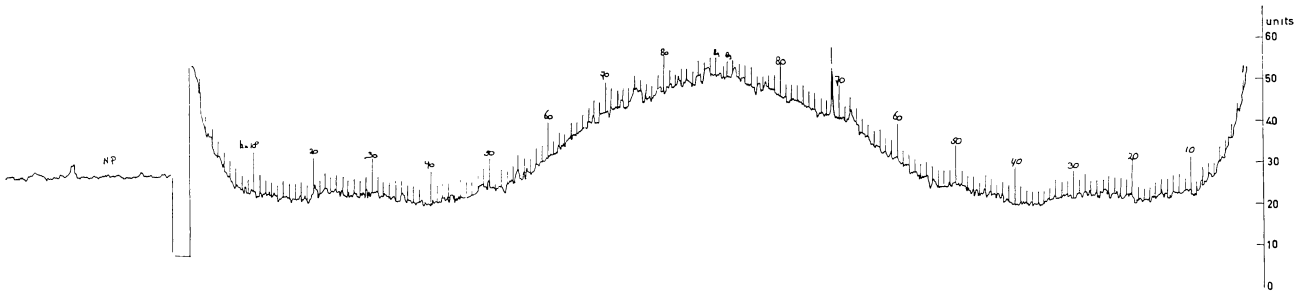

Figure 6. Sample record of a sweep in elevation, keeping right-ascension constant ($\alpha = 180°$), from $h = 0°$ to 90° and back to 0°.

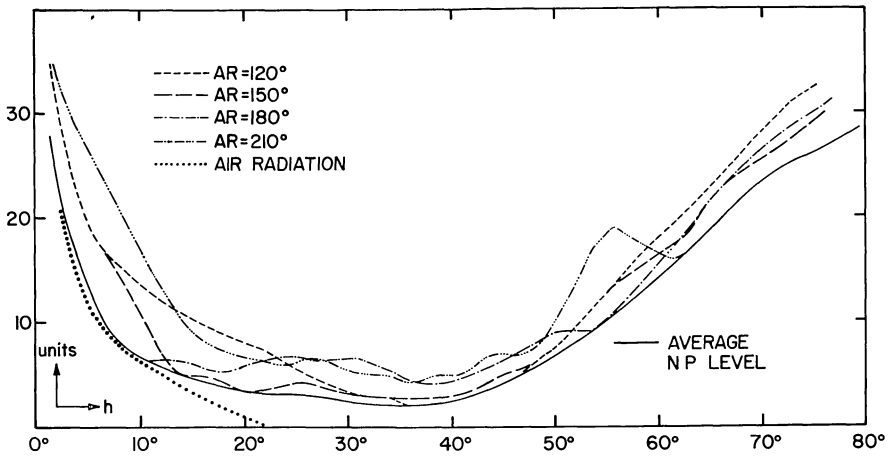

Figure 7. Four elevation sweeps, their lower envelope (solid line) and the expected air radiation. The lower envelope gives the total side-lobe and air radiation as a function of elevation.

210°. Figure 7 shows these four curves and the lower envelope. With the exception of a few regions with somewhat higher intensity, most of these curves go through regions where the intensities are very low, as can also be seen on the maps in figure 12. We estimate that the lower envelope gives the radiation from the ground and the air to within 3 units, relative to an arbitrary zero level. The average North Pole level for all 56 measurements is indicated in figure 7. It gives the intensity at $Az = 180°, h = 52°.8$, which is 0.6 units lower than the intensity given by the curve at $Az = 0°$, $h = 52°.8$. From a number of sweeps in elevation made at $Az = 180°$ (region D, see section 3.2) we find that the general shape of the lower envelope in the north is the same as that at $Az = 0°$. The data were too scarce, however, to include them in our standard curve.

It will be shown later (section 3.2) that the level of the curve with respect to the North Pole, as indicated in figure 7, is incorrect. It was determined in section 3.2 by studying the levels in the region of overlap with region A at $\delta > 35°$.

We shall now briefly discuss the shape of the curve. A perfect antenna with no side-lobes, looking at an empty sky, will as soon as the main beam has left the ground see only the radiation from the air coming into the main beam. If, as before, the extinction in the zenith is p and the extinction at zenith distance z is $p^{F(z)}$, the brightness temperature of the air can be written as

$$T_b(z) = T[1-p^{F(z)}],$$

where T is the weighted mean of the air temperature. If we put, more or less arbitrarily, $T = 250$ °K, and take $\log p = -0.0046$, we find that $T(z)$ decreases from 63 °K at $h = 2°$ through 21 °K at $h = 5°$, 15 °K at $h = 10°$ and 5 °K at $h = 30°$ to 3 °K at $h = 90°$. These are obviously rough values, since the weighting of T changes somewhat with h, but they indicate that most of the change in intensity at low elevation is due to air radiation. In figure 5, the dotted curve gives the air radiation expressed in our units, using the relation 1.2 °K in $\overline{T}_b = 1$ unit. For exact comparison, it would have to be smoothed over the antenna beam; this was not done, however. The rise of the intensity at altitudes above 40° must be due to the effect of far side- and back-lobes looking at the ground.

The semi-angle of the reflector, as seen from the feed, is 55°. Therefore, if the sensitivity of the feed is still considerable at the edge of the dish, a ring-shaped side-lobe will be formed between 90° and 125° from the main beam. One would expect that at low elevations, when half of this side-lobe is looking at the ground, not much change of ground-radiation with altitude will occur. But between elevations 50° and 90° more and more of this ring-lobe will be seeing the ground and we expect a considerable increase of intensity. The observed increase corresponds at least qualitatively with this effect. We may calculate the antenna sensitivity in this side-lobe by using the observation that between the zenith, when all of it looks at the ground, and low elevations, when only half does, the intensity increases

by roughly 30 units, equivalent with $\overline{T}_b = 36$ °K. If the full beam were looking at the ground it would observe the full ground temperature, say 250 °K. The effective solid angle subtended by the upper half of the ring-lobe thus is $\frac{36}{250}\,\Omega' = 0.76$ square degrees, or 1.52 square degrees for the entire lobe. If it were 30° wide, it would have a solid angle of about 8000 square degrees. Thus, writing $1.52 = f(\theta, \varphi) \times 8000$, we find that the antenna sensitivity $f(\theta, \varphi)$ is 0.019 per cent or 37.2 db below the sensitivity along the axis. This is unusually high, as in fact the unusual rise of the ground-radiation intensity indicated. The details of the antenna pattern are discussed in sections 1.3 and 1.4.

3. The main survey

It was planned to make all measurements in the form of right-ascension sweeps at constant declination, close to the meridian. Since radiation from the Sun in the far side-lobes prevented any measurements during the daytime, and the actual observing period was only seven weeks, observations had to be made at many different azimuths in order to cover the whole sky. The rather large variations in ground-radiation with elevation made it necessary to restrict the observations to sweeps at constant or nearly constant elevation. The fact that the telescope is alt-azimuth mounted has helped greatly in programming the observations such that large base-level variations during the sweeps were avoided. Even so, some variation of ground-radiation with azimuth occurred. The results proved, however, that, as could be anticipated, an alt-azimuth system is the most suitable for any observations where large areas of sky have to be mapped.

During the observing period, the amount of night-time hours decreased from 12 to about 10.

Since motorized traffic in a 1-km zone around the telescope was severely restricted, and the nearest main road is at 6 km distance, only occasional interference from ignition systems was experienced. The most serious source of interference was signals from radio sondes which occasionally had their transmission frequency in our receiving band. From direction-finding experiments it was concluded that they originated probably in Belgium and England. Approximately 20 per cent of the night-time hours was lost because of this interference. Occasionally, very-short-duration voice communication from military aircraft caused interference, but the shortness of the transmission periods made this type of interference not serious. Both sources of interference caused recorder deflections many times those from the Milky Way and were easily recognizable.

3.1. *Description of the observations*

Region α. Undoubtedly the best and most easily reduceable observations were made in the region between $\alpha = 90°$ to 270° and $\delta = +40°$ to $-32°$. Sweeps in α of 35° length were made at constant δ. The observing time was chosen such that the sweeps crossed the meridian and thus the elevation did not change by a large amount. Each sweep crossed two of the meridional sweeps described in section 2.3, which provided two tie-in points for zero-level determination. Short markers were automatically placed on the record every degree in α, with every 10 degrees a longer marker. At least two sweeps, in opposite directions, were made at each declination, and the declination interval was 1°. Sweep speeds were 8° or 4° per minute, depending on the gradient of the curves.

Region A. A very convenient way of referring all intensities in a region to the level of one point is making sweeps through the celestial North Pole. By sweeping back and forth between azimuths 80° and 280°, at an elevation of 52°.8 (latitude of Dwingeloo), curved tracks are made through the region between $\delta = 90°$ and 35°, each track going through the North Pole. The available observing time made it necessary to limit the azimuth coverage to 200° rather than 360°, which would have extended the region to $\delta = 15°.6$. The region between $\alpha = 0°$ and 90° was only partially covered because of the restriction of night-time observations only. Sweep speed was 13° per minute in azimuth, corresponding to 8° per minute on the sky. Azimuth markers were provided every 1° and 10°, and sidereal time was recorded every four minutes. Since one sweep back and forth required 31 minutes, adjacent sweeps during one night were about 6° apart. By choosing suitable starting times each night, and observing for seven nights, a coverage of one sweep on the average every degree in each direction was obtained. Near the North Pole the sweeps were of course very closely spaced, but this redundancy was necessary in order to obtain the common zero-level.

Regions B and C. In order to cover, in the time available, the areas not covered in regions α and A,

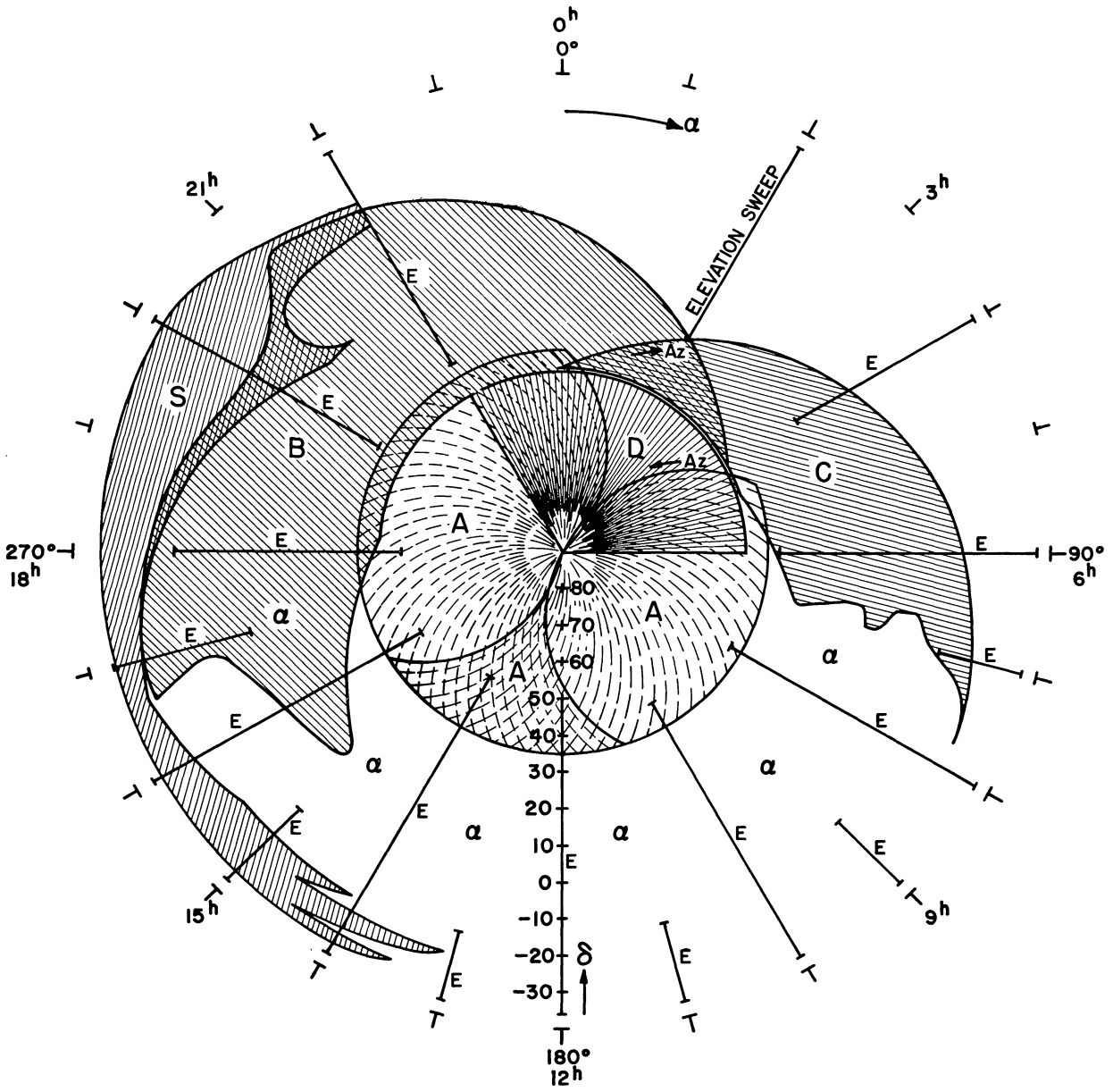

Figure 8. Polar map of the sky from declination +90° to −35°, giving the limits of the various regions described in section 3.

azimuth sweeps were made at an elevation of 10°, covering various intervals in the azimuth range 210°–330° (region B) and 20°–150° (region C). As shown in figure 8, these sweeps covered the declination range $\delta = +41°$ to $-27°$. The azimuth and time intervals were chosen such that the observations approached the region of the sky in which the Sun was situated as closely as possible, so that as much sky coverage as possible was obtained, without making daytime observations. The proximity of the Sun made observations in the region around $\alpha = 30°$ impossible. The sweep speed was 9°.3 per minute; azimuth and time markers, and degree of coverage, were the same as for region A. Both the sweeps at constant right-ascension,

and the region of overlap with region A could be used for the establishment of a zero-level.

Region S. Sweeps in azimuth at an elevation of 5° were made to fill in the part of the sky near the galactic centre, not covered by region B, and extending down to $\delta = -32°$. The sweeps were extended over a wide range of azimuths (260° to 50°) in order to provide sufficient overlap with regions B and α. Azimuth and time markers were the same as for region A; the average coverage near the galactic plane was very dense, approximately one sweep every 0°.2 in declination. Sweep speed was 8° per minute.

Region D. Since it was not possible to cover the whole North Polar cap with the region A sweeps, one night was spent making sweeps in elevation from $h = 0°$ to 52°.8 and back near azimuth 180°. By moving in azimuth at a suitable rate, these sweeps are sweeps in declination similar to the ones made near the meridian in the south. These sweeps cover the declination range $\delta = 40°$ to 90° between $\alpha = 330°$ and 90°. Every 1° in α a double sweep was made. The sweep speed was 18° per minute.

By employing three different methods of observation, it was possible to cover the whole visible sky, with the exception of a small region around the Sun, in a period of six weeks, using night-time hours only. All of the observed regions were covered at least twice, at intervals of at most 1° or one-half beamwidth. Many parts of the sky were covered considerably more densely. We estimate the total observing time, needed to cover the sky between $\delta = +90°$ and $-32°$ as 300 hours, not counting time lost through interference. This amounts to approximately three minutes per full beam area (5.3 square degrees).

3.2. *Method of reduction*

The measurements in regions A and D, the North Polar cap, were reduced first, and all other regions were referred to the zero-level of region A. All region A sweeps go through the North Pole; instrumental zero-lines could therefore be drawn immediately on the records. The intensities with respect to this zero were then read, multiplied with the appropriate gain correction factor, and tabulated as a function of azimuth. Since the elevation was constant, there is a unique relation between Az and δ, and between sidereal time and α for one Az. It was, therefore, simple to produce curves of intensity as a function of α, for constant δ, by plotting the intensities at one azimuth versus sidereal time and then shifting the ordinate by a constant amount to give α. This procedure was also followed for regions B, C and S. In these latter regions, corrections for differential extinction between the elevations of these regions and 52°.8 were also applied. Region D sweeps were read as a function of declination, and then combined into curves at constant δ. Region α sweeps, finally, were already in the form of curves at constant δ and were read at intervals of 1° in α.

All intensities were eventually referred to the intensity at the celestial North Pole, which was arbitrarily set at 10 units. We shall now discuss the determination of the final zero levels in each of the regions.

Region A. Sweeps between $Az = 80°$ and 180° and sidereal times 16^h and 18^h, and sweeps between $Az = 180°$ and 280° and sidereal times 8^h and 11^h, overlap around $\alpha = 210°$. The curves at constant δ derived separately from these two overlapping sets were shifted with respect to one another. This must be attributed to changes in the radiation coming in through

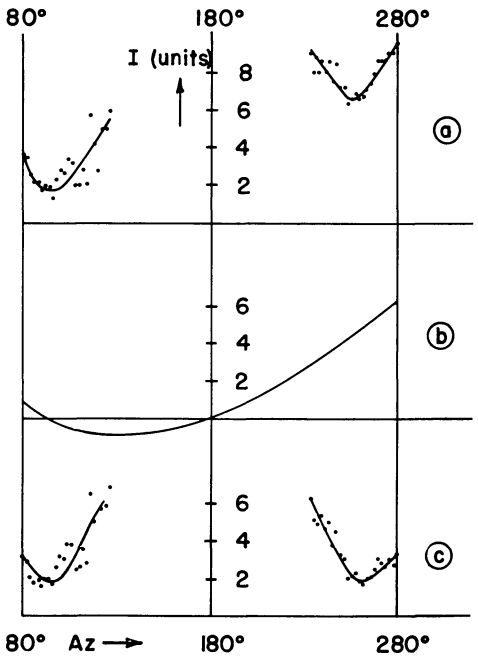

Figure 9. Side-lobe radiation with azimuth in region A. a) Uncorrected, b) Correction curve, c) Corrected. Intensities in a) and c) are averaged between $\alpha = 205°$ and 215°, and declination increases from $Az = 80°$ to 180° and from 280° to 180°.

the side-lobes with azimuth and time. The azimuth effect was first studied, by plotting the average intensity over 10° in α around $\alpha = 210°$ versus azimuth (via declination, figure 9a). Fortunately, a rather prominent minimum appeared in the background emission around $\alpha = 210°$, $\delta = 45°$. The two curves in figure 9a are in essence a declination cross-section through this feature; they should be mirror images of one another, $Az = 180°$ being the reflection point. A suitable choice of the distribution curve of side-lobe radiation as a function of azimuth (setting the side-lobe radiation at the North Pole equal to zero, figure 9b) results in corrected curves (figure 9c) which are exact mirror images. The curve in figure 9b is of course a rough approximation and has been drawn as smoothly as possible with the aid of the available data: the difference between the minima at $Az = 100°$ and 260°, the difference in the slopes on both sides of the minima, and the requirement that it should go through 0 at $Az = 180°$.

With the aid of this curve, the measurements were corrected by adding a constant amount, depending on the azimuth, to each intensity curve at constant declination (the one-to-one correspondence between azimuth and declination due to the method of sweeping at constant elevation made this correction very simple). It will be shown below that this first correction was insufficient, and that the main correction is a function of time rather than azimuth.

Region D. There was reasonable agreement between the lower envelope of the curves measured in region D, and the curve representing the radiation from the ground and the air (section 2.3). We therefore assumed that we could use this curve in the north as well as in the south, where it was measured. It was thus possible, since this curve gives the difference between the side-lobe radiation at the elevation of the North Pole and other elevations, to correct the curves of intensity versus altitude to curves of intensity versus declination, referred to the North Pole level. Corrections were made for extinction, receiver gain, and refraction and telescope setting errors.

As may be seen from figure 8, there is a certain amount of overlap of regions A and D. When the curves of intensity versus right-ascension for the two regions were compared, it was found that in the interval $\alpha = 50°$–90° the region A intensities were higher than the region D intensities by 1 to 1.5 units. In the interval $\alpha = 330°$–360°, however, region A intensities were lower than region D intensities by as much as 11 units at $\delta = 90°$. It could be shown, by comparison with regions B and C, that this was due to a wrong zero-line correction with azimuth in region A, and probably hardly to changes in the shape of the side-lobe radiation curve with time in region D. The zero-levels of regions B and C were determined entirely from comparisons with region A in the region of overlap $\delta = 35°$–40°, and by using the declination curves at intervals of 30° in α as connecting links. The region B zero-level was entirely determined by the region A data from $\alpha = 270°$–4°. The zero-level of region C was interpolated between the region A overlap at $\alpha = 63°$–80° and $\alpha = 356°$–8°. A comparison of the levels of regions B, C, and D in the overlap interval of the three ($\alpha = 340°$–60°) showed that the same difference in level as was found between regions A and D existed between B and D, and persisted over the entire region D interval (figure 10a). This indicated that the level of region A in the interval $\alpha = 330°$–360° was lower by about 12 units at $\delta = 40°$ than the level of region A in the interval $\alpha = 50°$–90°. The region A measurements in the former interval were made around sidereal time 20^h ($Az = 180°$–280°), those in the latter around 8^h ($Az = 80°$–180°).

Since azimuth corrections had already been applied,

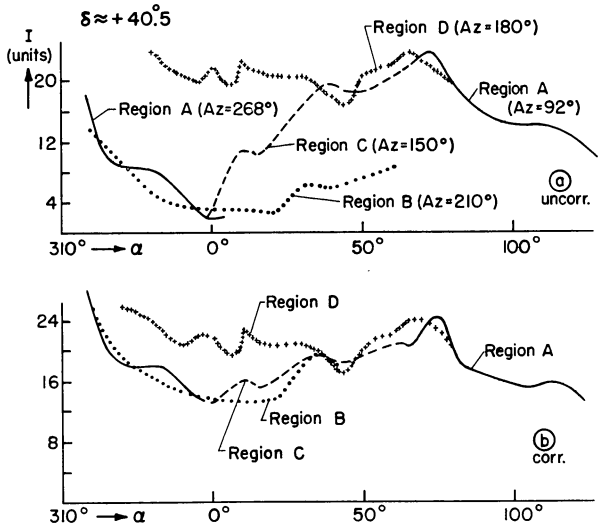

Figure 10. Intensities in regions A, B, C, and D as a function of α around $\delta = 40°.5$. a) Uncorrected for the change in side-lobe radiation with time, b) Corrected.

the only other explanation is a time effect in the side-lobe radiation. It was assumed to decrease, relative to the North Pole, at a rate of 0.68 units per hour at $\delta = 35°$. The effect was assumed to be the same in the two azimuth ranges 80°–180° and 280°–180°. The levels were adjusted such that they were equal in the overlap region $\alpha = 210°$, and in the overlap regions with region D there was reasonable agreement between A, B, C and D. The rate of change decreased from 0.68 units per hour at $\delta = 35°$ to 0 at $\delta = 90°$. The result is shown in figure 10b for one declination. It may be observed that between $\alpha = 330°$ and 30° the region D level is still too high; more value was attached, however, to the good agreement between regions A, B, and C, which were observed more carefully and frequently (region D was only observed on one night, and using a completely different method). At declinations above 41°, beyond which the regions B and C do not extend, the zero-levels of the region D measurements filling the gap between the two ends of region A were adjusted to fit the final region A levels.

We can now combine the two corrections to region A into one, giving the side-lobe radiation as a function of azimuth for different times (figure 11). The side-lobe radiation at the North Pole was kept equal to zero at all times. The shape of the curves looks highly artificial, in particular the sharp peak near the North Pole; this is mainly due to the assumption of symmetry with respect to $Az = 180°$ in the correction as a function of time. However, the available data did not allow a more precise determination. It might have been possible to try other possibilities giving more reasonable curves, but it was felt that the arbitrariness of this would not warrant the amount of work involved.

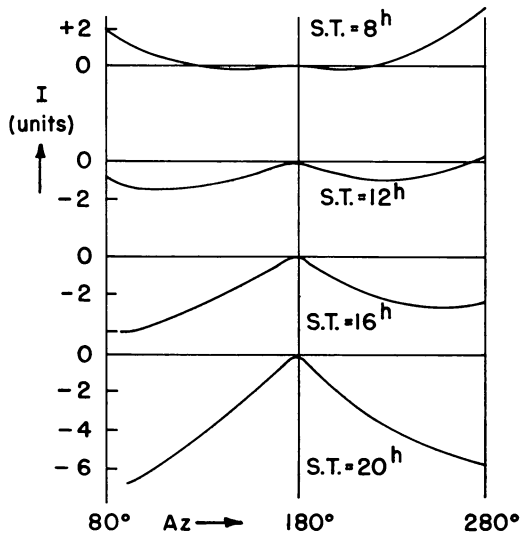

Figure 11. Side-lobe radiation with azimuth in region A at four different sidereal times.

It is of interest to investigate the origin of this variation in the side-lobe radiation. If we assume, as in section 2.3, that most of it comes into a ring-shaped lobe between 90° and 125° from the main beam, then the upper half of this lobe looks at the sky close to the horizon, sweeping from east through south to west when the telescope sweeps from $Az = 80°$ through 180° to 280°, but presumably covering an arc of horizon at least 90°, perhaps 180° long all the time. During the night the side-lobe radiation from the south (i.e., when the telescope is looking at the North Pole) seems to rise with respect to the side-lobe radiation from the east and the west. Qualitatively, this could be expected since the brighter parts of the Milky Way fill more and more of the southern sky when the sidereal time increases above 15^h. A very rough estimate could be made of the expected magnitude of the effect, taking the value of the antenna sensitivity $f(\theta, \varphi) = 1.9 \times 10^{-4}$ in the ring side-lobe, and assuming it to cover a solid angle of 8000 square degrees (section 2.3). Around 12^h sidereal time, the section of sky 60° on either side of the meridian has an average brightness of about 12 units, whereas around 20^h it has an average brightness of about 70 units. If outside the ring side-lobe, $f = 0.8 \times 10^{-4}$ in a solid angle of $90° \times 120° = 10800$ square degrees, and if the ring side-lobe looks at 2000 square degrees, then the difference in the side-lobe radiation between 12^h and 20^h would be

$$\begin{aligned} \Delta T_A &= \int fT \, d\Omega/\Omega \\ &= (0.8 \times 10^{-4} \times 60 \times 10800/9.4) \\ &\quad + (1.9 \times 10^{-4} \times 60 \times 2000/9.4) \\ &\approx 8 \text{ units}, \end{aligned}$$

which is of the right order of magnitude.

Another, perhaps equally important source of variation in the side-lobe radiation, might be a change in the effective ground temperature during the night. This might be brought about by the formation of dew on the flat ground to the south of the antenna during the night, a not uncommon phenomenon during the time

of the year in which the observations were made. A dew-covered area will have a considerably higher reflection coefficient than a dry area, and since the average sky temperature is far below the temperature of the ground, will have an effective temperature well below the ambient temperature. With the antenna pointing to the North Pole, much of the hypothetical ring lobe will see the wooded area to the east and the west of the telescope, where formation of dew is absent. Moving away from the north, one-half of the ring lobe sweeps across the flat area to the south, thus seeing an effective temperature which decreases during the night. It is impossible to make even a guess at the magnitude of the effect. However, a combination of both effects might well explain the overall shape of the variation in side-lobe radiation with time and azimuth.

We are inclined to believe that our correction, although certainly not perfect, has resulted in an internally consistent set of data, the overall level of which is probably off by no more than 5 units. The final result of this reduction is given as a contour map in polar coordinates covering all of the sky between $\delta = 35°$ and 90° (figure 12a). Most of the observations are those of region A, with additional information from regions B and C between 35° and 40°, and from region D around $\alpha = 350°$. All measurements below $\delta = 35°$ were referred to this polar cap.

Calibration sweeps at constant α. The sweeps, made in the southern meridian in order to determine the side-lobe radiation as a function of elevation (section 2.3) were freed from this by subtracting the standard curve (figure 7). The curves at $\alpha = 120°$, 150°, 180°, 210°, 240°, and 270° overlapped with region A, and the zero-level with respect to the North Pole could be determined. It was found on the average to be about 5–6 units below the average North Pole levels determined while the sweeps were made. As mentioned in section 2.3, these were very uncertain, but the fact that the differences were all of the same order might indicate a difference in side-lobe radiation between the south and the north, which was removed by using the overlap with region A as a standard. The intensities were corrected for extinction and gain variations, and the positions converted from elevation to declination, including instrumental and refraction corrections. The curves at $\alpha = 90°$ and $\alpha = 300°$ were tied to the standard system by comparison with regions C and B. The curves at $\alpha = 330°$, 30° and 60° were not used.

Regions B and C. Instrumental zero-levels were determined by comparing the intensities of the azimuths overlapping region A with the final region A intensities. In addition, region C, which does not overlap with region A over its full range, was compared with region B in its overlap region. In order to find a possible variation of side-lobe radiation with time and azimuth, the intensities were compared with the intensities of the curves at constant α intersecting the regions at $\alpha = 90°$, 240°, 270° and 300°. Since the region B and C measurements cross these curves at different azimuths and times, the differences could be plotted as functions of time and of azimuth. The curves at constant α which were not tied to region A showed a constant difference with region B or C over their entire length and their zero-level was accordingly corrected. The spread in the differences from point to point was $\pm$ 3 units; no systematic effects in time or azimuth were found. This could be due to two reasons: radiation from the ground in the side- and back-lobes is less severe at this elevation (10°), and the sweeps did not extend all the way to the north, where the side-lobe radiation seemed worst at 52°.8 elevation. More evidence for the absence of variation in side-lobe radiation came from comparison with region α, where it overlaps with regions B and C. Differences were never greater than $\pm$ 2.5 units. We conclude that the zero-levels of regions B and C do probably not deviate by more than 5 to 7 units from the level of the North Pole, hopefully considerably less.

Region S. The sweeps in region S covered the azimuth range $Az = 260°–50°$, and thus cross the meridian. It can easily be shown that in such a case each sweep has one point in common with each of a large number of following sweeps. This makes it possible to determine an internally consistent zero-level by comparing the intensities in the common points. Azimuth sweeps across the meridian are thus, like sweeps through the pole, excellently suited for surveys in which the instrumental zero-level cannot be easily determined. This procedure also largely eliminates possible effects of side-lobe radiation varying with azimuth and time and provides a net of sweeps in various directions through an area by moving the telescope in one coordinate only. The absolute zero-level was determined by comparison with region B in the

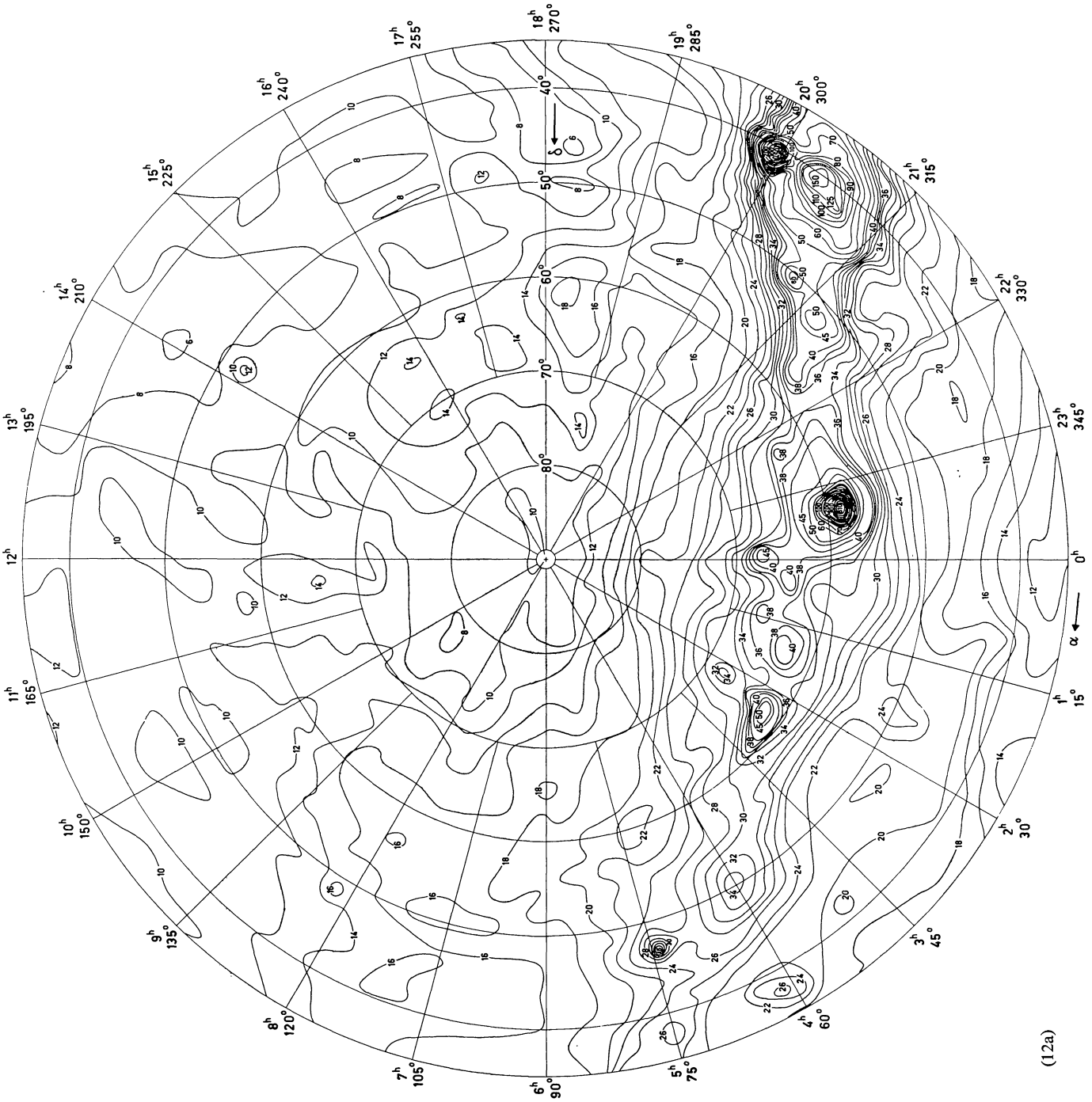

(12a)

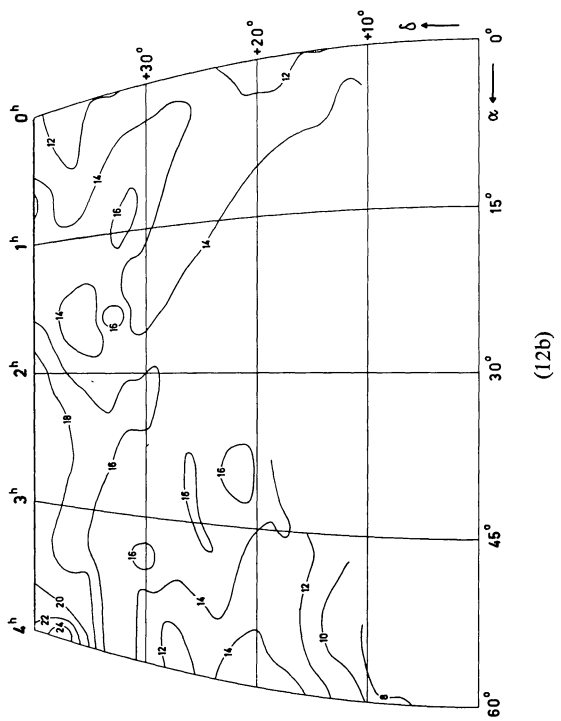

(12b)

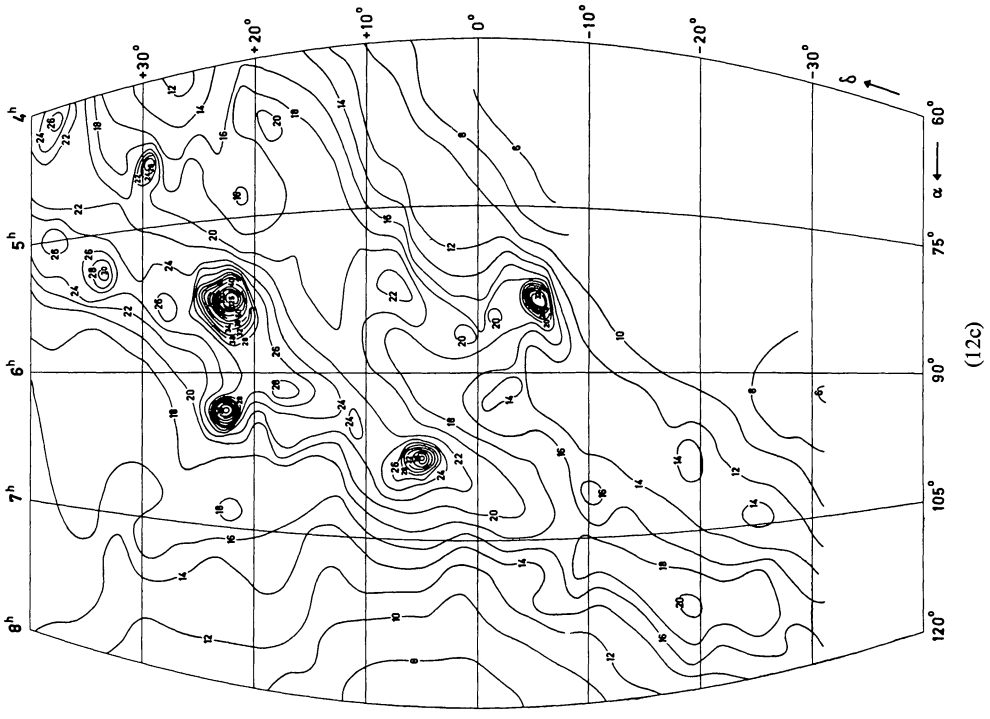

(12c)

Figure 12. Contour maps of the 400 Mc/s background radiation, in equatorial coordinates for 1950. Contours are labeled in units. T_A = $= 0.67 \times$(units+14); $\bar{T}_b = Q \times$(units+14) where $Q = 1.2$ for small regions (10 to 100×full beam) and 0.9 ± 0.2 for large regions (1/2 or 1/4 of sky).

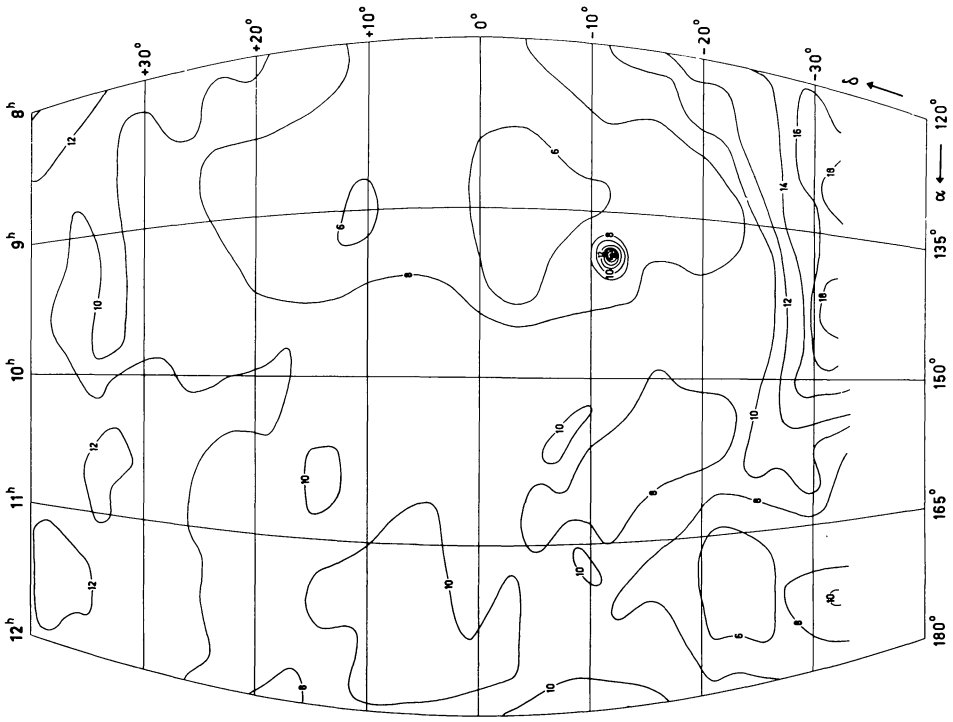

(12d)

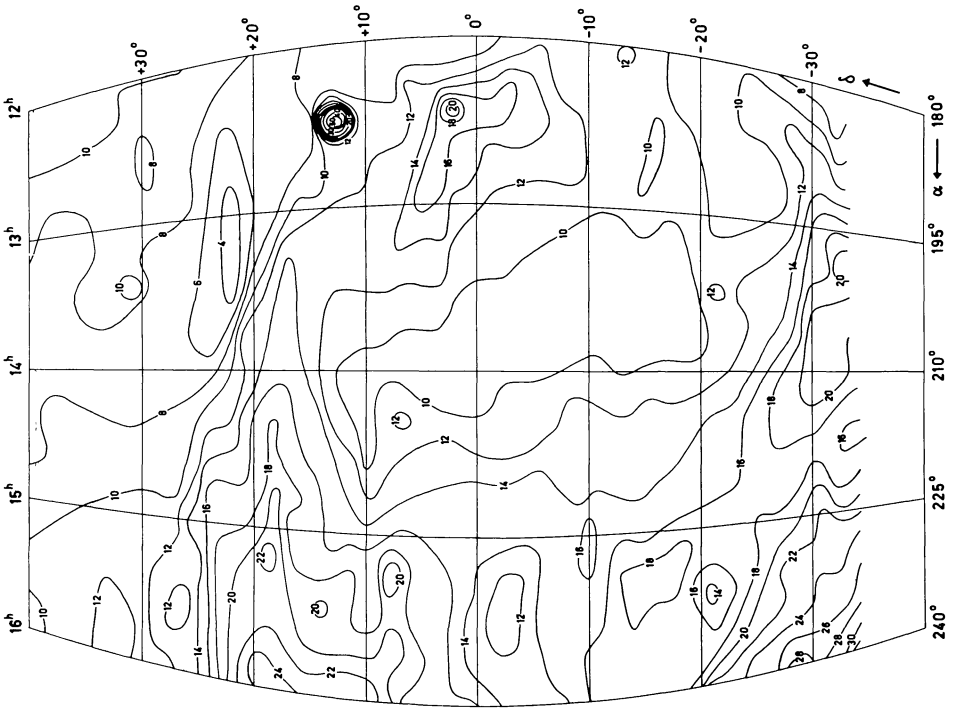

(12e)

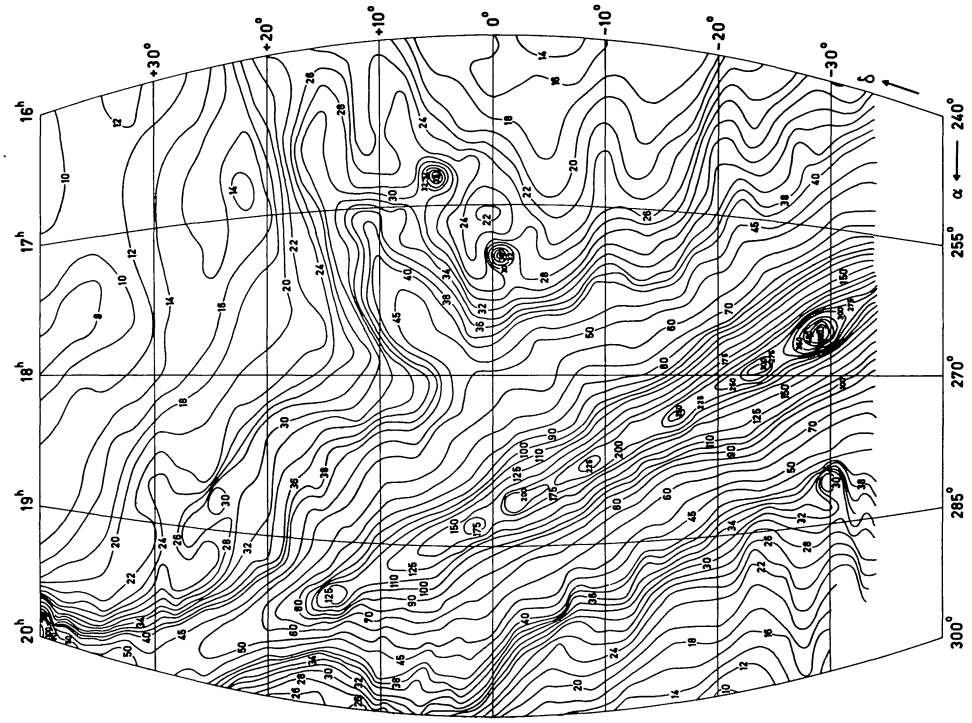

(12f)

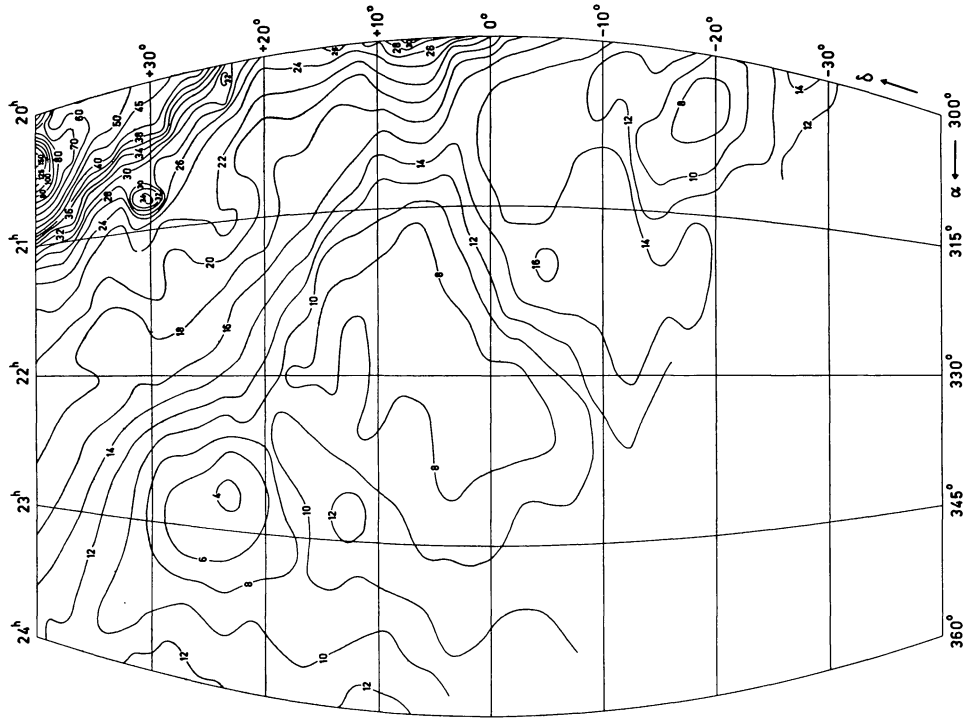

(12g)

overlap region, and with the curves at constant α at $\alpha = 210°$, 240° and 300°.

Extinction corrections were applied to reduce the intensities to those at elevation 52°.8 (factor 1.04 for regions B and C, 1.08 for region S). Refraction and instrumental effects in regions B, C and S were taken care of during the observations by setting the telescope such that the real elevation was 10° and 5°, respectively. The intensities of regions B, C and S were collected, as a function of α, into curves at constant δ.

Region α. The measurements, in the form of curves at constant δ, obtained by moving the telescope over 35° in right-ascension, were provided with zero-lines by comparison with the curves at constant α every 30° in α. The zero-lines were drawn on the recorder paper in the following way. First, the intensities of the two curves at constant α were read at the points where they crossed the region α sweep. Since the recorded measurements were not yet corrected for gain changes and extinction, these intensities were subjected to a reverse correction before plotting them in the appropriate place on the recorder paper. The measurements were not made at a constant elevation, and thus the zero-lines were in general not straight lines. They were drawn taking into account the differential side-lobe radiation at the varying elevation (elevation was automatically indicated every degree), obtained from the curve described in section 2.3. A semi-automatic curve reader was then employed to read the intensities with respect to this zero-line every degree in α. The curve reader electronically multiplied these intensities with the correction factor for gain and extinction and plotted the corrected intensities on graph paper. At least two measurements were made at each declination, and corresponding measurements were plotted on the same sheet of paper.

The sweeps below $\delta = 20°$ were made to cover only 15° at a time. The elevation changes for longer sweeps would cause badly curved zero-lines at these low elevations (elevations 5°.2 to 17°.2), where the side-lobe- and air-radiation increase sharply. To provide zero-levels at both ends of these short curves, additional curves at constant α were obtained at $\alpha = 105°$, 135°, 165°, 195°, 225°, and 255°. These curves only extended to about $\delta = -10°$ and their zero-levels were determined from the overlap with the region α sweeps between $\delta = -10°$ and $-20°$. The reduction procedure then was the same as that for the measurements with $\delta > -20°$.

3.3. *Contour maps*

From the reductions described above, curves were now available giving intensity as a function of right-ascension at intervals of 1° in declination for region α, and approximately 0°.7 in declination for the other regions. All zero-levels were referred to the level of the North Pole, which was arbitrarily set at 10 units to avoid negative intensities. Corrections were applied for extinction, refraction and instrumental effects, and the gain was standardized on the intensity of Virgo A, which was set at 50 units with respect to its comparison region. These curves were then converted into contour maps on equal-area charts for the interval $\delta = -32°$ to $+40°$ and on a polar coordinate chart for the interval $\delta = +35°$ to $+90°$. While copying these maps for publication, the coordinates were slightly shifted so that the maps in figure 12 are corrected for precession to 1950.

A one-degree galactic coordinate grid was drawn on the maps, and the contours were then transferred to a rectangular galactic map and two polar maps. The transfer was done by putting transparent paper on top of the equatorial maps and match the one-degree squares as well as possible. Close to the galactic equator this was very simple since on the equal-area charts the squares were practically not deformed. At higher latitudes, however, a considerable amount of fitting and measuring had to be done. Afterwards, it was realized that it would probably have been easier to construct completely new contour maps in galactic coordinates, by drawing an equatorial grid on the rectangular galactic grid and transferring contours from the curves at constant declination. This was actually done for the Cygnus region (around $\alpha = 20^h$, $\delta = +40°$) where complicated contours coincided with a rather deformed galactic grid. The maps in new galactic coordinates are presented in figure 16, at the end of the paper.

4. Discussion

4.1. *Comparison with Cambridge*

A survey of the sky with a 7°.5 beam at 404 Mc/s was made at the Mullard Radio Astronomy Observatory (PAULINI-TOTH and SHAKESHAFT, 1962), in Cambridge. In this survey, particular attention was paid to the accurate calibration of the receiver and to the corrections for radiation received in side-lobes. It is

believed that the accuracy of the brightness temperature is of the order of $\pm$ 1 °K and the absolute background level is known to about $\pm$ 2 °K. A comparison of this survey with ours will thus lead to a determination of our background level, which is unknown (the North Pole level was set arbitrarily at 10 units). Also, it will be possible to compare the brightness temperature scales of the two surveys.

The comparison was made as follows. First, since both surveys use the North Pole level as a standard, these levels were made equal by finding x for the North Pole in $\overline{T}_b$ (Dwingeloo) = 1.2 (10 units + x) = $\overline{T}_b$ (Cambridge) = 23.9 °K, assuming our scale factor 1 unit = = 1.2 °K in $\overline{T}_b$ is correct. This leads to x = 10 units. Using this, we may convert our units into units of $\overline{T}_b$ in °K above a zero background, $\overline{T}_b$ = 1.2 (units + 10) °K (long dashes in figure 13).

We compared the cross-sections at constant declination, tabulated by the Cambridge group, with cross-sections from our contour maps. The Cambridge values were converted from their tabulated T_a' to T_b using the procedure outlined in their paper (full-drawn curves in figure 13). In figure 13, five sample cross-sections, at intervals of 20° in declination, and two cross-sections at constant right-ascension are given.

It is clear from figure 13 that the general agreement between the two surveys is satisfactory. The differences amount to no more than 6 °K or 5 units, with very few exceptions. Of course, the deviations along the brighter parts of the galactic equator are larger, due to the difference in beamwidths. However, the level of our survey is systematically higher than that of the Cambridge survey in the region between $\alpha = 8^h$ and 13^h, brought out especially in the two lower curves, at $\alpha = 9^h$ and 12^h. This is the region of lowest intensities, where, as mentioned in section 1.4, the brightness temperature is expected to be more nearly equal to the antenna temperature (η_B closer to unity) and thus the conversion factor between our units and $\overline{T}_b$ should be smaller than 1.2, perhaps 0.8 or 0.9. Since the North Pole is already close to this region, the calculation of x above should be made using a conversion factor smaller than 1.2. We arbitrarily assume that at the North Pole it is 1.0, which leads to x = 14 units. We adopted this as the zero-level correction, and calculated the cross-sections again with

$\overline{T}_b$ = 1.2 (units + 14) °K (crosses in figure 13).

There is good agreement between these and the Cambridge cross-sections in the more intense parts of the sky. For the flat low-intensity parts, we calculated cross-sections with

$\overline{T}_b$ = 0.9 (units + 14) °K (small dashes in figure 13).

Clearly, the large deviations between 8^h and 13^h were

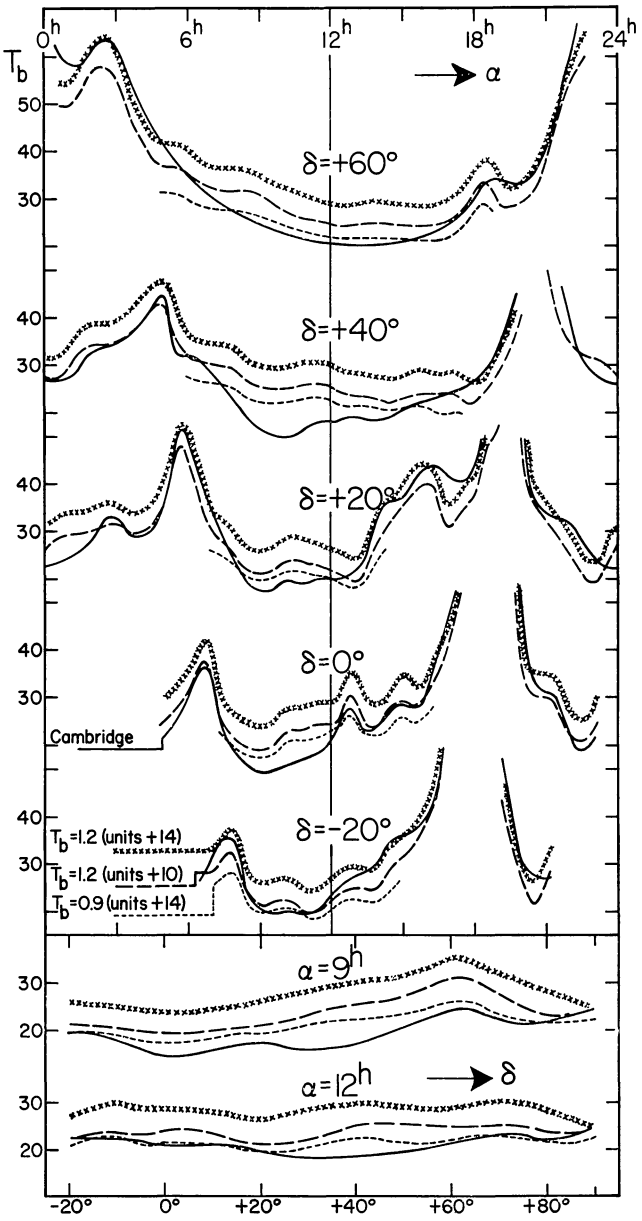

Figure 13. Comparison of our survey with the Cambridge survey. Cross-sections in α at five values of δ, and in δ at two values of α.

mainly due to the use of a wrong conversion factor.

We can now draw the following conclusions from this comparison:

a) All intensities in the contour maps have to be raised by 14 ± 5 units in order to be proportional to the actual antenna temperature due to extra-terrestrial radio emission.

b) Antenna temperature and our units are related by

$$T_A = 0.67\,(\text{units}+14)\ ^\circ\text{K}\,.$$

c) The value of the beam efficiency, η_B, depends on the size of the region under consideration. For details of size similar to that of the full beam (to within a factor of 10 or 100) $\eta_B = 0.56$. For larger details, η_B will increase, up to perhaps 0.8 for details with size of the order of $\frac{1}{4}$ to $\frac{1}{2}$ of the sky.

d) Since $\overline{T}_b = \dfrac{1}{\eta_B} T_A$, the relation between our units and $\overline{T}_b$ depends on the size of the region under consideration. It is found that good agreement with the Cambridge survey is obtained by using

$$\overline{T}_b = 1.2\,(\text{units}+14)\ ^\circ\text{K}$$

for small details (sources, galactic plane), and

$$\overline{T}_b = 0.9\,(\text{units}+14)\ ^\circ\text{K}$$

for larger low-intensity regions, with conversion factors somewhere in between for regions of intermediate size.

4.2. *Ratios of bright sources*

During the course of the survey, many measurements were made of the intensities of Cas A, Tau A, Vir A and Cyg A. These intensities were measured with respect to a comparison region (see section 2.2) and intensity ratios were determined for each group of measurements made within a short period of time. In those cases where one source was consistently at a lower elevation than the others (which happened mostly with Vir A), extinction corrections were applied. A weighted mean of the ratios over the entire observing period was made, the weight of each ratio being the product of the number of observations of each of the two sources. This resulted in two groups of ratios, one determined from the data used for the daily gain measurements throughout the observing period, the other from the extinction measurements made during two short periods. The ratios were subsequently corrected for the non-linearity of the receiver using the values derived close to the days of observation rather than the average approximate value of p derived in section 1.2. The uncorrected and corrected values, and their average, are given in table 4. The large difference (3 per cent) in the ratios Cas A/Vir A is unexplained, but does raise some doubts about the reality of the probable errors.

In order to find the ratios of the flux densities, it is necessary to determine the difference in intensity between the comparison regions and the background underlying the source. Since most of the sources are in the neighbourhood of the galactic ridge, the uncertainty in the background determination is rather large. The intensities with respect to the comparison region were obtained by multiplying the standard intensity of Vir A, 50 units, with the average ratio from table 4. In table 5, the values used for the comparison region and the background, the intensity with respect to the background, the ratio of the intensity to that of Vir A and Cas A, and the flux density, taking $S(\text{Cas A}) = 5600 \times \times 10^{-26}$ watt $\cdot$ m^{-2} $\cdot$ (c/s)$^{-1}$ are given. The source number from the following paper (Davis *et al.*, 1965) is also given.

The intensity of Sgr A is an average obtained by using the extinction measurements, and the numerous

Table 4

Ratios of five bright sources with respect to their comparison regions

	From daily measurements			From extinction measurements			Average ratio
	Ratio		Weight	Ratio		Weight	
	uncorrected	corrected		uncorrected	corrected		
Cas A/Vir A	11.34 ± 0.05	11.70 ± 0.11	531	11.07 ± 0.10	11.34 ± 0.13	135	11.63 ± 0.15
Tau A/Vir A	2.34 ± 0.02	2.35 ± 0.03	454	2.31 ± 0.10	2.33 ± 0.11	105	2.35 ± 0.03
Cyg A/Vir A				8.94 ± 0.17	9.10 ± 0.20	222	9.10 ± 0.20
Cyg X/Vir A				3.07 ± 0.07	3.09 ± 0.08	204	3.09 ± 0.08

TABLE 5

Ratios and fluxes of six bright sources

Source	No.	I (units) (source-comp.)	comp.	background	I (units) (source-backgr.)	$\frac{I\text{ (source)}}{I\text{ (Vir A)}}$	$\frac{I\text{ (source)}}{I\text{ (Cas A)}}$	Flux density $[10^{-26}\text{W} \cdot \text{m}^{-2} \cdot (\text{c/s})^{-1}]$
Cas A	148	581.5 ± 7.5	42	32 ± 5	591.5 ± 10	11.83 ± 0.20	1.000	5600
Tau A	25	117.5 ± 1.5	18	26 ± 2	109.5 ± 3	2.19 ± 0.06	0.185 ± 0.005	1036 ± 28
Vir A	57	50	9	9 ± 1	50.0 ± 1	1.00	0.085 ± 0.002	476 ± 10
Cyg A	129	455.0 ± 10.0	14	45 ± 8	424.0 ± 13	8.48 ± 0.26	0.717 ± 0.022	4015 ± 125
Cyg X	134	154.0 ± 4.0	24	50 ± 5	128.5 ± 7	2.57 ± 0.14	0.217 ± 0.012	3740*
Sgr A	96	527 ± 10	40	310 ± 15†	257 ± 20	5.14 ± 0.40	0.434 ± 0.033	3040**

* Assuming an apparent size of 3°.5 × 3°.5 (see following paper, DAVIS *et al.*, 1965).
** Assuming an apparent size of 2°.5 × 2°.0.
† Corrected for receiver alinearity.

region S measurements from which the contour maps were prepared. Extinction and non-linearity corrections were applied. The background in the contour maps was estimated at 305 ± 15 units, and was corrected for non-linearity before entering the value into the table.

The intensities given in table 5 are slightly different from those in the contour maps. This is due to the fact that the contour maps were not corrected for non-linearity. As mentioned earlier, the non-linearity correction is so small that only for the five brightest sources, and for the Milky Way between $l^{II} = 0°$ and 52° does it amount to more than 0.5 per cent.

In December 1960, during the 408 Mc/s polarization measurements (WESTERHOUT *et al.*, 1962), a series of measurements was made to determine whether any change in the source ratios had occurred in the 3.5 years since the ratios in table 4 were determined. This is of interest since it is known that the flux density of Cas A decreases with time. The ratio of the intensities with respect to the comparison regions was found to be Cas A/Tau A = 4.93 ± 0.10 in 1960, as compared to 4.95 ± 0.07 (from table 4) in 1957. This would indicate a constant ratio; however, the ratio Tau A/Vir A = 2.24 ± 0.06 in 1960, as compared to 2.35 ± 0.03 in 1957. Since we do not expect the intensities of Tau A and Vir A to change by 5 per cent in 3.5 years, this decrease indicates that the ratios determined in this way cannot be compared. The reason probably is that the antenna pattern in 1960 differed considerably from that in 1957 and thus the difference in intensity between background and comparison region was different. Unfortunately, no determination of the background underlying the sources was made in 1960, so that a comparison of true flux density ratios could not be made. We judge the equality of the Cas A/Tau A ratios in the two years as fortuitous. The experiment indicates that in order to find flux density changes of the order of 1 per cent, identical antennas should be used and great care has to be taken in the determination of the background intensity.

4.3. *The galactic ridge and spur*

In the regions where the original azimuth sweeps cross the galactic equator and the 'spur', the azimuth, elevation and intensity of the maximum were determined. After correction for gain, extinction and zero-level, and conversion of the coordinates to l^{II}, b^{II}, the maximum intensities were plotted as a function of l^{II} for the galactic ridge and of b^{II} for the spur. Also, the values of b^{II} and l^{II}, respectively, were plotted (figures 14 and 15). In this way, all available points are plotted rather than the smooth averages from which the contour maps were prepared, and an accurate determination can be made of the position of the ridge line. Such a determination was not made here, but it is evident from the lower part of figure 14 that the distribution is symmetrical with respect to the new galactic equator.

As KERR (1962, his figure 10) has already noted, some 'steps' are visible in the distribution of the radiation with longitude. The most noticeable steps occur at $l^{II} = 80°$ and at $l^{II} = 49°$, where the line of sight passes through a long stretch of the Orion arm and the Sagittarius arm, respectively. MILLS (1959) was the first to point out the existence of such steps in the continuous radiation, and concluded that they indicate the presence

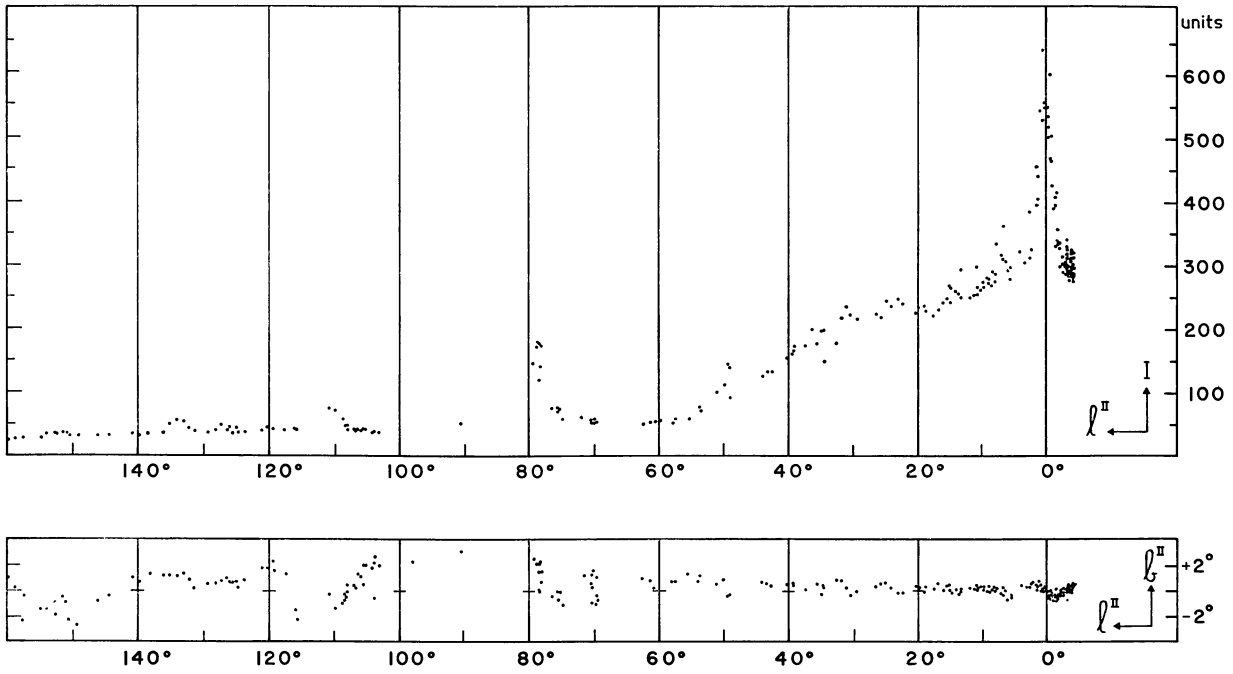

Figure 14. Intensity and latitude of the galactic ridge.

of a spiral structure in the continuum emission. KERR (1962) points out that there is good agreement between the positions of spiral arms determined in this manner, using both radio and optical data (ELSÄSSER and HAUG, 1960), and the neutral hydrogen arms determined using the 21-cm line data. We feel that the two above-mentioned steps are the only cases in our survey where one has some evidence for this conclusion. It is, however, quite easily possible to draw a smooth line through the points in figure 14 without any step-like features, except for the region near $l = 80°$, which is due to the complicated Cygnus-X region. Although a model in which a considerable fraction of the non-thermal emission is concentrated in the spiral arms is attractive, such a model is not necessary to explain the distribution of the radiation with longitude, neither in our survey nor in any other. The 'steps' could equally well be explained as small irregularities, since they represent deviations from a smooth curve of only 10 to 20 per cent.

The reason for plotting the data for the 'spur' (figure 15) is to show the relative smoothness of this feature. Most remarkable is the constancy of the galactic longitude of the ridge line. Over the latitude range from $b^{II} = +15°$ to $+48°$, the longitude does not deviate by more than 2° from $l^{II} = 32°$ ($l^{I} = 359°.7$). At higher latitudes, the ridge begins to deviate from a great circle. It passes the north galactic pole at a latitude of about 75°, and can be followed easily over more than 90°; it is still clearly visible just south of Vir A, at $\alpha = 12^h15^m$, $\delta = -5°$. LARGE *et al.* (1962) note that the parts visible in our survey fit remarkably well to a small circle of diameter $111° \pm 5°$ centred on $\alpha = 15^h 00^m \pm 10^m$, $\delta = -36° \pm 2°$. In a recent series of papers, HASLAM *et al.* (1964) present a complete survey of the spur at a frequency of 240 Mc/s, using a beamwidth of $1°.4 \times 1°.0$. Since their survey, convolved to our beamwidth, agrees in detail with ours, we refer for a discussion of the detailed structure of the spur to their paper.

4.4. *Polarization of the background radiation*

After the reductions of the present survey were made, it was discovered that the background radiation was partially linearly polarized (WESTERHOUT *et al.*, 1962). Study of the complete sky map showing the intensity and direction of the linearly polarized component (BERKHUIJSEN and BROUW, 1963) shows that in most of the sky the intensity is of the order of 2 °K or about

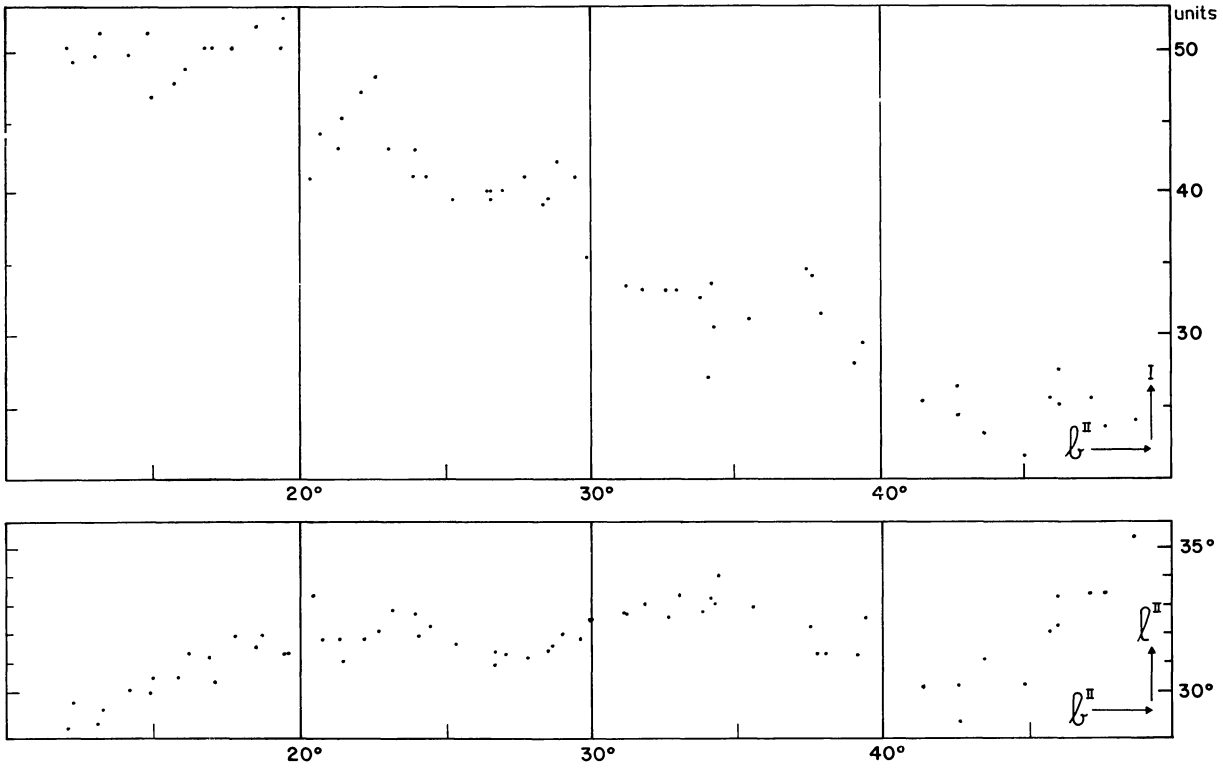

Figure 15. Intensity and longitude of the 'spur'.

2 units, or smaller. In view of the other uncertainties, associated with the side-lobe radiation, this has no appreciable influence on the final accuracy of the contour maps.

In two regions, the polarized component is of the order of 5 °K: around $l^{II} = 0°$, $b^{II} = 60°$, an area of about $15° \times 15°$; and between $l^{II} = 125°$ and 171°, $b^{II} = 0°$ and 20°.

Since the antenna was vertically polarized at all times, measurement of a polarized region will give different results depending on the orientation of the electric vector with respect to the antenna. Neither of the regions from which the side-lobe corrections as a function of azimuth and time were determined (by comparing observations of the same region at different times, section 3.2) coincides with the regions of strong polarization. Thus, polarization effects in these corrections are small compared to the side-lobe radiation.

In the region $l^{II} = 125°$ to 140°, $b^{II} = -10°$ to $+15°$ (part of region D) the antenna polarization was more or less parallel to the background polarization, so that the maximum effect might be expected. As a result, the intensities in that region are probably too high by about 3 units, relative to the intensities received with an (imaginary) unpolarized antenna (i.e., half the intensity of the polarized component). It might be that the bulge in the contours around $l^{II} = 130°$, $b^{II} = +8°$ is due to this, and conceivably even the source near that position (source no. 10 in the following catalogue) might be spurious, although its size is somewhat too small (3°) with respect to the region concerned. In the region around that mentioned above, where the polarized component is still of the order of 6 or 7 units, its position angle with respect to the antenna was between 40° and 90°; the resulting increase in the general level will be smaller than 2 units, and therefore negligible.

In the region around $l^{II} = 0°$, $b^{II} = 60°$, which was observed in our region α survey, the direction of polarization of the antenna with respect to the equatorial coordinate system differed by more than 45° at different declinations, and for different measurements at the same declination, due to different times of observation. In some cases, it was parallel to the direction of the polarized component, in other cases perpendicular.

Most of the polarized component was averaged out when averaging different measurements, and it is estimated that the maximum effect of the polarized component on the contour maps is less than 2 units and thus negligible.

4.5. *Conclusion*

A survey is presented which is believed to represent the distribution of antenna temperature over the sky with an estimated probable error of $\pm$ 5 units (3.4 °K in T_A) in the zero-level and $\pm$ 5 per cent in the relative temperature scale. Relative brightness temperatures can be calculated with an accuracy of $\pm$ 5 units (6 °K in $\bar{T}_b$) for large extended regions. The absolute temperature scale is tied into the flux density of Cas A, and is estimated to be accurate to within $\pm$ 15 per cent.

One of the most remarkable features of the radio sky, brought out by this survey, is the highly irregular structure away from the galactic plane. The spectrum of this part of the sky is characteristic of the synchrotron mechanism, so that we are led to the conclusion that most, if not all of the radiation is due to the presence of relativistic electrons and a magnetic field in this region. The so-called 'halo' radiation seems to come from an assembly of very large extended sources, rather than from a smooth medium. It is interesting to note that the radiation from the galactic plane between $l^{II} = 0°$ and 60° is relatively smooth, whereas the galactic plane between $l^{II} = 90°$ and 240° has much the same general irregular appearance as the 'halo'. In the case of the galactic plane radiation, this difference can be explained by the fact that the line of sight in the directions $l^{II} < 60°$ goes through at least 15 kpc of emitting material, and even if this is distributed in the form of extended sources, the result will be rather smooth. For $l^{II} > 90°$, the line of sight goes through perhaps 5 kpc of a less dense medium, and irregularities show up because a much smaller number of components contributes to the total radiation. This then leads to the question whether the 'halo' is perhaps much less extended than previously assumed. The standard picture of the 'halo' is that of a rather smooth medium, more or less spherically distributed, with a radius to half-density points of the order of 10 kpc. In most directions in the region $l^{II} < 90°$ therefore the line of sight should go through at least 10 kpc of emitting material and one would expect a much more smooth distribution than observed. The irregularities in the present survey might well be interpreted as being due to relatively nearby 'clouds' of emissive material. A similar conclusion was reached earlier in connection with a discussion of the polarized component of the galactic background radiation (WESTERHOUT, 1964). The emissive material in the 'halo' might thus be much closer to the galactic plane than hitherto assumed, perhaps within 1 or 2 kpc. It might be connected with it through violent activities within the plane, such as the removal of material by very strong supernova outbursts.

The direct connection between the galactic plane and the 'halo' material is strongly suggested by such features as the 'spur' at $l^{II} = 32°$ (which is clearly part of an arc) in the north galactic hemisphere and the 'Cetus arc' (LARGE *et al.*, 1962) (of which our survey shows the two ends at $l^{II} = 45°$ and $l^{II} = 155°$) in the south galactic hemisphere. There is an indication in our survey of 'spurs' of a similar nature, though less pronounced, emerging from the galactic plane to the north at $l^{II} = 88°$ and $l^{II} = 155°$. In fact, with some imagination, one might connect these two features as another arc which reaches its highest point at $l^{II} = 130°$, $b^{II} = +50°$. Each of these 'arcs' is suggestive of the occurrence in or close to the galactic plane of an explosive phenomenon, the effect of which is visible in those regions where no resistance by heavier interstellar matter is encountered. Other 'extended sources', which together provide the remainder of the radiation at higher galactic latitudes, may be the remnants of older 'arcs', now broken up.

No explanation has been found for the deep minima rather close to the plane, at $l^{II} = 25°$, $b^{II} = -28°$ and $l^{II} = 90°$, $b^{II} = -32°$. Similar minima, although less pronounced, occur at the same latitude north of the plane. A very peculiar minimum of almost the same dimensions as the antenna beam, at $l^{II} = 6°$, $b^{II} = -12°$, can probably be explained as a freak combination of the steep gradient of the background emission and two small discrete sources (Nos. 107 and 116 in the following article).

Acknowledgements

The authors are grateful to Professor Ir. C. A. Muller and his staff at the Dwingeloo Observatory, without whose help the successful completion of this survey

would not have been possible. They are pleased to thank Mr. J. H. Kuypers and Mrs. J. Westerhout for their assistance in the observations, and Messrs. I. Robbers and P. H. Kiel for their share in the tedious reductions.

References

W. Altenhoff, P. G. Mezger, H. Strassl, H. Wendker and G. Westerhout, 1962, *Veröff. Univ. Sternw. Bonn* **59**

E. M. Berkhuijsen and W. N. Brouw, 1963, *Bull. Astr. Inst. Netherlands* **17** 185

C. C. Cutler, 1947, *Proc. Inst. Radio Eng.* **37** 1284

M. M. Davis, L. Gelato-Volders and G. Westerhout, 1965, *Bull. Astr. Inst. Netherlands* **18** 42

H. Elsässer and U. Haug, 1960, *Z. Ap.* **50** 121

C. S. Gum and J. L. Pawsey, 1960, *Mon. Not. Roy. Astr. Soc.* **121** 123

C. G. T. Haslam, M. I. Large and M. J. S. Quigley, 1964, *Mon. Not. Roy. Astr. Soc.* **127** 273

F. J. Kerr, 1962, *Mon. Not. Roy. Astr. Soc.* **123** 327

M. I. Large, M. J. S. Quigley and C. G. T. Haslam, 1962, *Mon. Not. Roy. Astr. Soc.* **124** 405

B. Y. Mills, 1959, *Symp. I.A.U.* **9** 431

I. I. K. Paulini-Toth and J. R. Shakeshaft, 1962, *Mon. Not. Roy. Astr. Soc.* **124** 61

E. Schoenberg, 1929, *Handbuch der Astrophysik*, ed. G. Eberhard, A. Kohlschutter and H. Ludendorff (Verlag Julius Springer, Berlin) **2** 268

Ch. L. Seeger, G. Westerhout and H. C. van de Hulst, 1956, *Bull. Astr. Inst. Netherlands* **13** 89

Ch. L. Seeger, 1956, *Bull. Astr. Inst. Netherlands* **13** 100

Ch. L. Seeger, G. Westerhout and R. G. Conway, 1957, *Ap. J.* **126** 585

Ch. L. Seeger, F. L. H. M. Stumpers and N. van Hurck, 1960, *Philips Techn. Rev.* **21** 317

J. R. Shakeshaft, M. Ryle, J. E. Baldwin, B. Elsmore and J. H. Thomson, 1955, *Mem. Roy. Astr. Soc.* **67** 106

G. Westerhout, 1958, *Bull. Astr. Inst. Netherlands* **14** 215

G. Westerhout, Ch. L. Seeger, W. N. Brouw and J. Tinbergen, 1962, *Bull. Astr. Inst. Netherlands* **16** 187

G. Westerhout, 1964, *Symp. I.A.U.* **20** 139

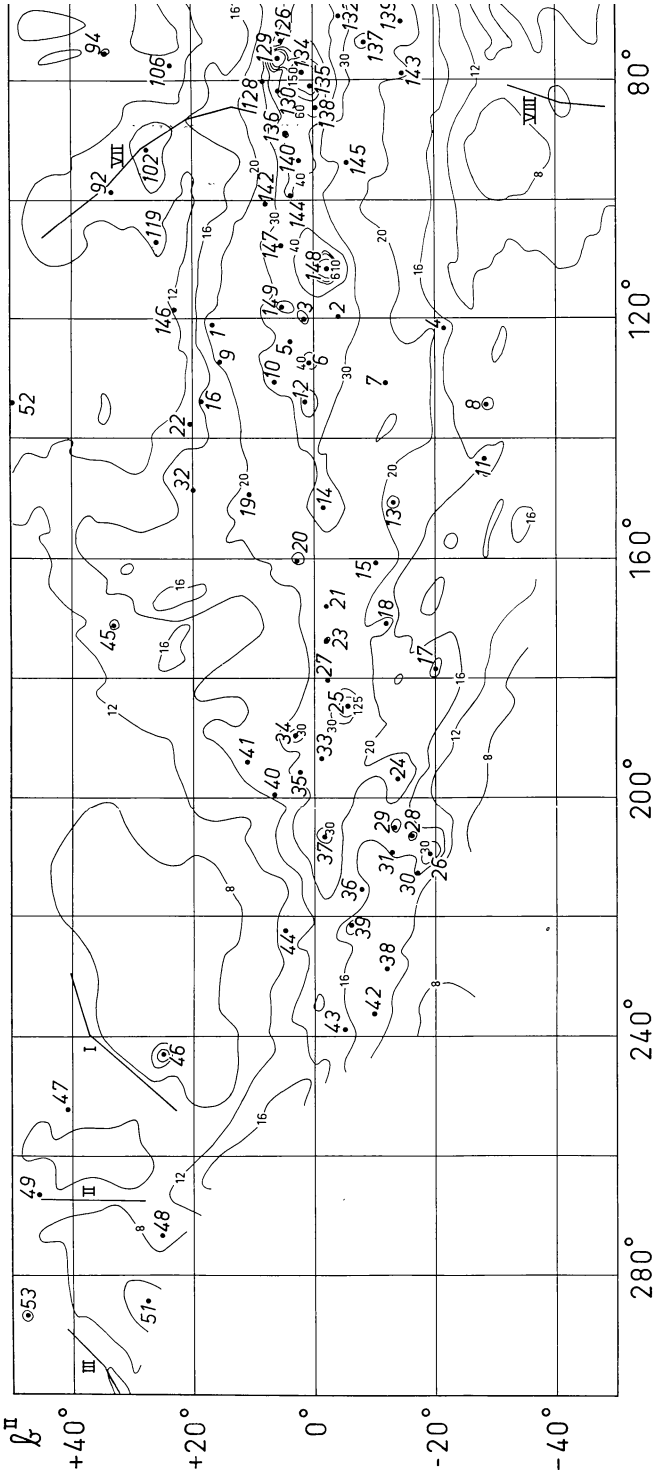

1965BAN....18...11S

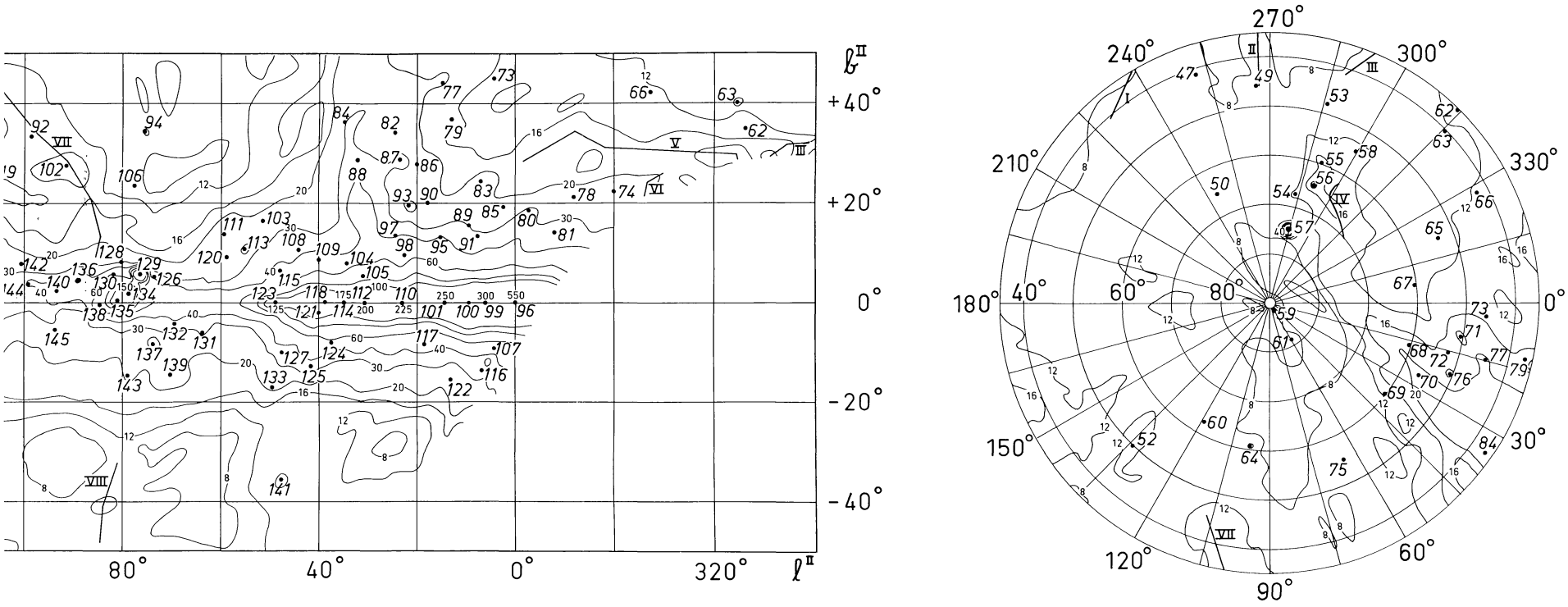

Figure 1. Finding chart for 'ridges' (table 2) and sources (table 3). The contours of the background radiation have been taken from paper I.

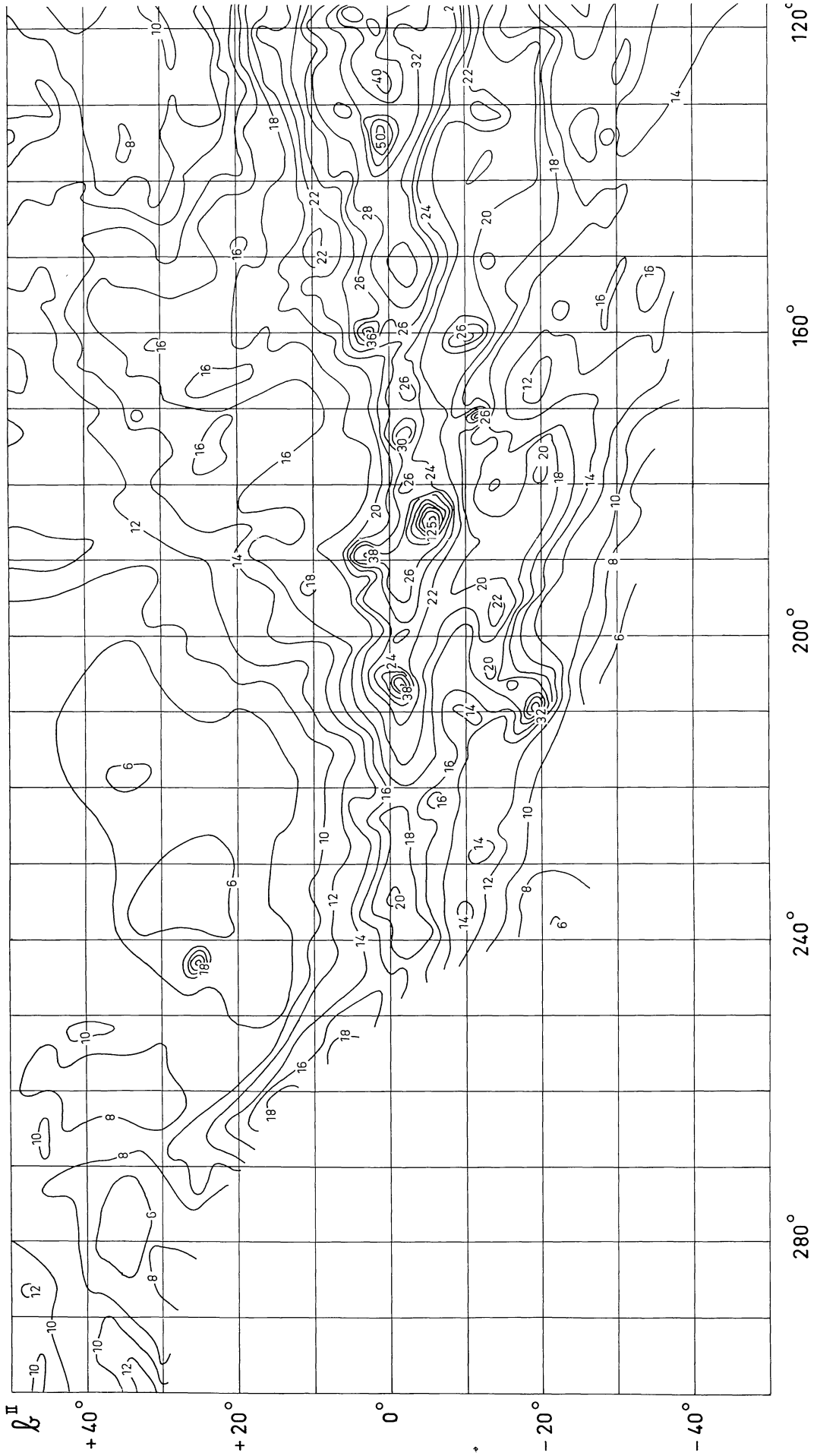

Figure 16 (Seeger *et al.*). Contour maps of the 400 Mc/s background radiation, in new galactic coordinates. Contours are labeled in units. $T_A = 0.67 \times (\text{units} + 14)$; $\bar{T}_b = Q \times (\text{units} + 14)$ where $Q = 1.2$ for small regions (10 to 100 × full beam) and 0.9 ± 0.2 for large regions (1/2 or 1/4 of sky).

1965BAN....18...11S